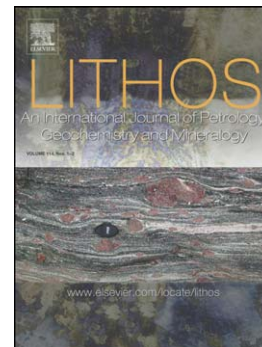# Accepted Manuscript

Origin of Mafic and ultramafic cumulates from the Ditrău Alkaline Massif, Romania

Elemér Pál-Molnár, Anikó Batki, Enikő Almási, Balázs Kiss, Brian G.J. Upton, Gregor Markl, Nicholas Odling, Szabolcs Harangi

Please cite this article as: Pál-Molnár, Elemér, Batki, Anikó, Almási, Enikő, Kiss, Balázs, Upton, Brian G.J., Markl, Gregor, Odling, Nicholas, Harangi, Szabolcs, Origin of Mafic and ultramafic cumulates from the Ditrău Alkaline Massif, Romania, *LITHOS* (2015), doi: 10.1016/j.lithos.2015.09.022

ORIGIN OF MAFIC AND ULTRAMAFIC CUMULATES FROM THE DITRĂU ALKALINE MASSIF, ROMANIA

Elemér Pál-Molnár[a,b,+], Anikó Batki[b,*], Enikő Almási[a], Balázs Kiss[b], Brian G.J. Upton[c], Gregor Markl[d], Nicholas Odling[c], Szabolcs Harangi[b]

[a] Vulcano Research Group, Department of Mineralogy, Geochemistry and Petrology, University of Szeged, Egyetem Street 2, H-6722 Szeged, Hungary, e-mail: palm@geo.u-szeged.hu

[b] MTA-ELTE Volcanology Research Group, Pázmány Péter Street 1/C, H-1117 Budapest, Hungary, e-mail: batki@geo.u-szeged.hu,

[c] School of GeoSciences, University of Edinburgh, Grant Institute, The King's Buildings, James Hutton Road, Edinburgh EH9 3JW, United Kingdom

[d] Fachbereich Geowissenschaften, Universität Tübingen; Wilhelmstrasse 56, D-72074 Tübingen, Germany

* Corresponding author.

[+] The first two authors have contributed equally to this work.

Abstract

Mafic–ultramafic cumulates enclosed in gabbroic–dioritic rocks form part of the Mesozoic Ditrău Alkaline Massif in the Eastern Carpathians, Romania. The poikilitic olivine-and pyroxene-rich and nearly mono mineralic hornblendite rocks display typical cumulate textures with early crystallised olivine (Fo_{75-73}), diopside and augite. In the early stages of their genesis the amphibole was intercumulus while in later stages it acquired cumulus status as the fractionating magma evolved. Using major and trace element compositions of minerals and whole-rock samples the origin of these cumulates is determined and the parental magma composition and depth of emplacement are calculated.

Cumulus clinopyroxene has more primitive composition than intercumulus amphibole suggesting closed system fractionation for the evolution of poikilitic olivine-and pyroxene-rich cumulates. The evolution of the amphibole-rich mesocumulates is more clearly the result of closed system crystallisation dominated by the precipitation of clinopyroxene and amphibole cumulus crystals.

Lamprophyre dykes of the Ditrău Alkaline Massif are proposed to reflect multiple basanitic parental magma batches from which the cumulus olivine and clinopyroxene crystallised.

Relative to these dykes the calculated equilibrium melts for intercumulus amphibole in the cumulates was more primitive whilst that for the cumulus amphibole was more evolved. The calculated crystallisation temperature and pressure of ~1000–1050 °C and ~0.7 GPa, based on the composition of the amphiboles, indicate crystallisation at lower crustal depths. Rare earth element compositions are consistent with an intra-plate tectonic setting.

Keywords

Mafic–ultramafic cumulate; Laser ablation; Thermobarometry; Intra-plate magmatism; Ditrău Alkaline Massif

1. Introduction

Mafic-ultramafic cumulates are also common in intra-plate alkaline igneous complexes, but amphibole-rich cumulates are relatively rare in such settings (e.g. Gardar Province, South Greenland (Upton et al., 1996), Monteregian Hills, Canada (Eby, 1984)). In contrast, large volumes of amphibole-rich cumulate rocks are abundant in middle to lower crust of volcanic arcs (Davidson et al., 2007). The formation of amphibole-rich cumulates in arc settings is well studied both empirically and experimentally (e.g. Larocque and Canil, 2010; Krawczynski et al., 2012; Tiepolo et al., 2012; Smith, 2014). Ultramafic and mafic rocks are widespread in the Dinarides and the Carpathians and represent components of ophiolite complexes (Hoeck et al., 2006). However, not all are of ophiolitic origin and some, with the Ditrău mafic–ultramafic cumulates being an example, represent within-plate intrusions that contain amphibole-rich lithologies (e.g., hornblendites) (Morogan et al., 2000; Pál Molnár, 2000). The Ditrău mafic–ultramafic rocks are predominantly hornblendite cumulates (Morogan et al., 2000; Pál-Molnár, 1992, 2000, 2010b). Generalised descriptions of these ultramafic bodies have been extensively reported over the past 150-years (e.g. Bagdasarian, 1972; Batki et al., 2014; Codarcea et al., 1957; Dallmeyer et al., 1997; Fall et al., 2007; Herbich, 1859; Ianovici, 1933, 1938; Jakab, 1998; Kräutner and Bindea, 1998; Mauritz, 1912; Mauritz et al., 1925; Morogan et al., 2000; Pál-Molnár, 1992, 1994, 2000, 2010b; Pál-Molnár and Árva-Sós, 1995; Streckeisen, 1952, 1954, 1960; Streckeisen and Hunziker, 1974), but none of these studies have considered their mineral scale petrology, petrogenesis and *P–T* conditions of cumulate formation in detail. New petrography, whole-rock and mineral chemistry data are presented in this paper and are used to assess the crystallisation history, the depth of formation of the ultramafic cumulates and their petrogenesis.

2. Geological setting

The Ditrău Alkaline Massif is a Mesozoic igneous complex in the Eastern Carpathians of Romania (Fig. 1A). The massif outcrops immediately east of the Călimani–Gurghiu–Harghita Neogene–Quarternary volcanic chain (Fig. 1B) and is partly covered by andesitic pyroclasts and lavas and by Pliocene–Pleistocene sediments (Codarcea et al., 1957). It is sub-circular in plan (19 km x 14 km) covering, ~200 km^2 (Pál-Molnár, 2000). The massif consists of a series of ultramafic and mafic rocks grading into intermediate and felsic rocks from west to east. Hornblendite, amphibole-bearing gabbro and diorite are the dominant rock-types in the north- and central-west part of the massif (Fig. 1C, D). Monzonite, syenite, quartz syenite and granite occur in the north, the south and the south-east, while nepheline syenite is concentrated in a large area of the central and the eastern part (Fig. 1C). The whole complex is cut by numerous dykes including camptonites, tinguaites, alkali feldspar syenites and nepheline syenites.

The Ditrău Alkaline Massif intruded during an extensional phase of the Alpine orogeny, related to a rifted continental margin adjacent to Tethys. Intrusion of the magmas is inferred to have been related to the opening events of Meliata–Hallstatt ocean (Hoeck et al., 2009), where rifting began in the Pelsonian Substage (Middle Triassic) (Kozur, 1991).

The Massif lies within the Dacia Mega-Unit of the Alpine–Carpathian–Dinaric region (Fig. 1A) and intrudes the Variscan metamorphic rocks that form the Alpine Nappes in the Eastern Carpathians (Săndulescu, 1984). Alpine nappes were thrust over each other in the Cretaceous (Austrian tectogenesis), and have an eastern vergence. From bottom to top the following nappes were identified by Săndulescu (1984): Infrabucovinian, Subbucovinian and Bucovinian (Fig. 1B). Each nappe is composed of Pre-Alpine metamorphic rocks and Permian-Mesozoic sequences, with the youngest formation being older than Late Albian. Structurally, the massif is the part of the Bucovinian Nappe, having direct contact with four of its Pre-Alpine lithogroups (Pál-Molnár, 2010a). All of the above mentioned sequences are intruded by the massif.

The ultramafic rocks were the earliest components, emplaced at 216–237 Ma, although their age overlaps that of the gabbros (234 Ma). The nepheline syenites and granites are somewhat younger (216–232 Ma and 196–217 Ma respectively). Original dating was by K/Ar on hornblende, biotite, nepheline and feldspar separates, (Pál-Molnár and Árva-Sós, 1995) and a mid- to late-Triassic age of the early components was subsequently confirmed by additional ^{40}Ar/^{39}Ar hornblende ages of 231 Ma and 227 Ma for gabbro and diorite, respectively

3

(Dallmeyer et al., 1997). A mantle origin for the mafic and ultramafic bodies was inferred by Kräutner and Bindea (1998) and Morogan et al. (2000).

3. Field relationships and samples

The mafic–ultramafic cumulates crop out in the north- and central-west part of the massif. They are enclosed in gabbroic–dioritic rocks as lenticular or block shaped bodies from a few centimetres to hundred metres or more in size (Tarniţa Complex, Pál-Molnár 2000) – see Figure 1 of the Online appendix. The enclosing gabbroic and mainly dioritic rocks and enclosed cumulates have almost the same mineral compositions (clinopyroxene, amphibole, plagioclase, biotite and accessories). Changes in modal % of minerals can result different rock types even in hand specimen scale. Continuous grading from hornblendite to gabbro, diorite, monzodiorite, monzonite, quartz monzonite, syenite, quartz syenite and granite can be observed from the north-west to the north-east part of the massif despite the fact that there are age differences. Although the massif is cut by several smaller faults, the grading can be observed in a horizontal traverse from west to east through 9 km along Jolotca Creek (Fig. 1C). Thus, the rock sequence in the north-west to the north-east part of the massif is inferred to be tectonically tilted. The ultramafic rocks are the lowest in the sequence relative to all the other rock units.

The mafic–ultramafic cumulates are composed of dense mineral phases, thus they are interpreted to have originated as vertical successions built up on the chamber floor. The massif was uplifted and most likely tectonically tilted from its original vertical position during the Alpine (Bucovinian) nappe formation.. Boreholes in the massif have penetrated to depths of 1200m yet have not reached the Subbucovinian Nappe under the Bucovinian Nappe (Kräutner and Bindea, 1995) and therefore, any information on the crustal depth of the original rock mass can only be obtained from thermobarometry.

Samples of the mafic–ultramafic cumulates were collected in the north-west part from eleven outcrops at Jolotca, Csibi-Jakab, Pietrăriei de Jos, Pietrăriei de Sus, Tarniţa de Jos, Tarniţa de Sus, Ascuţit and Filep Creeks (Fig. 1D).

4. Petrography

The igneous cumulate suite of Ditrău Alkaline Massif is notable for its petrologic diversity. The rocks are dark grey, coarse-grained and inequigranular orthocumulates and mesocumulates. The mafic–ultramafic rocks cover a wide spectrum from those in which olivine and/or clinopyroxene are dominant to those that are essentially mono-mineralic

4

hornblendite (up to 91% amphibole, Fig. 2A). Two major types can be recognised based on the texture: 1. poikilitic olivine-rich cumulate in which amphibole occurs as an intercumulus phase and 2. amphibole- and pyroxene-rich cumulates with cumulus amphibole crystals. It is important to note that olivine-bearing cumulates are quite scarce. Despite careful field and petrologic investigations, only a few occurrences have been recognised throughout the massif. Olivine and pyroxene are always cumulus minerals (Fig. 2). Biotite and plagioclase, when present, are confined to the intercumulus. Amphibole (100 μm – 11mm) occurs both as a cumulus and intercumulus phase.

Pokilitic olivine-rich cumulates have up to 30 modal% olivine, 23% euhedral cumulus clinopyroxene and scarce orthopyroxene enclosed by large intercumulus amphibole oikocrysts (Fig. 2B and D). Olivine occurs as subhedral to anhedral cumulus crystals (up to 1.7 mm) enclosing primary magnetite. Fresh olivine is uncommon as it is extensively replaced by serpentine and magnetite showing mesh structure (Fig. 2B). Clinopyroxene is found as microcryst, with crystal size of 150–600 μm. The accessory phases are apatite and magnetite. Orthopyroxene is always rounded, strongly cracked and surrounded by a fine-grained reaction rim of 40–50 μm thickness consisting of talc, subordinate plagioclase and rarely magnetite (Fig. 2C). This disequilibrium texture points to a xenocrystic origin for the anhedral orthopyroxene. It is most probably a localised product of side-wall contamination. The xenocrysts are up to 750 μm and contain magnetite inclusions.

Amphibole- and pyroxene-rich cumulates consist of amphibole, pyroxene, plagioclase, biotite, magnetite, titanite and apatite. These rock types are dominated by cumulus amphibole crystals with variable grain size. In single samples it occurs as euhedral to subhedral macrocrysts up to 11mm across (Fig. 2B, E and H) and also as subhedral crystals, 100–500 μm in size, described here as microcrysts (Fig. 2A and F). Amphibole oikocrysts (>10 mm) commonly enclose clinopyroxene, titanite, magnetite and apatite crystals and often display a sagenitic texture. Some show marginal alteration to chlorite and epidote. Euhedral to subhedral clinopyroxene comprises up to 16 modal%. This clinopyroxene commonly encloses amphibole and is often partially pseudomorphed by secondary amphibole and chlorite or epidote (Fig. 2D and E). It is rarely zoned, occurs as macrocrysts up to 4 mm in size (Fig. 2D), and also occurs enclosed in amphibole oikocrysts with sizes of around 450 μm. Subordinate biotite (1–20%) is subhedral with clinopyroxene, amphibole, apatite and magnetite inclusions, can reach 4 mm in size and commonly marginally chloritised. In some cases, intergrowths of biotite and amphibole indicate their simultaneous formation but where biotites – up to 4 mm – enclose amphibole and clinopyroxene they are clearly of later origin.

5

Subhedral to anhedral intercumulus plagioclase (up to 12%) occurring between the mafic components also contains clinopyroxene inclusions (Fig. 2F and G) and shows sericite alteration. Apatite (up to 5%), magnetite (up to 5%) and titanite (up to 3%) occur both as intergranular crystals between major components (Fig. 2 G and H) and as inclusions in the cumulus crystals suggesting their early saturation. Euhedral to subhedral titanite crystals up to 2 mm in size (Fig. 2G) contain apatite and magnetite inclusions. Apatite occurs as euhedral crystals. Calcite rarely occurs next to titanite. Magnetite crystals are rounded or anhedral, sometimes associated with apatite or zircon (Fig. 2). The sequence of crystallisation is inferred to be olivine, clinopyroxene, amphibole, biotite and plagioclase with continuous and increasing apatite, magnetite and titanite formation.

4. Analytical methods

Four hundred and ninety electron microprobe measurements were performed on selected olivine, orthopyroxene, clinopyroxene, amphibole, biotite and plagioclase crystals. Analyses were made with a Cameca SX-50 electron microprobe in wavelength-dispersive mode at the Institute of Geological Sciences, University of Bern, Switzerland, using a beam current of 20 nA and an acceleration voltage of 15 kV and at the Institut für Geowissenschaften, Universität Tübingen, Germany, using a JEOL 8900 electron microprobe in wavelength-dispersive mode operated at an acceleration voltage of 15 kV and a beam current of 15 nA. Counting times were 16s for peak and 8s for background measurements. Standards used were both natural and synthetic mineral phases. Processing of the raw data was carried out with the internal $\phi\rho z$ correction method of JEOL (Armstrong 1991) and using online PAP Cameca Software.

In order to measure the trace and rare earth element concentrations in the main ferromagnesian minerals, 16 amphibole, 12 clinopyroxene and 2 olivine grains from 5 polished thin sections were analysed.

Laser ablation ICP-MS analyses were carried out at Cardiff University, using a New Wave Research UP213 Nd-YAG 213 nm UV laser system coupled to a Thermo X Series 2 ICP-MS. All measurement were made using Thermo Elemental PlasmaLab time-resolved analysis mode. The laser beam diameter was 40 μm, with a frequency of 10 Hz and a power of ~3.5 J cm^{-2}. Ablations were carried out under a pure helium atmosphere. Acquisitions lasted about 90 s, including a 20-s gas blank prior to the start of the analysis and a 10-s washout at the end. BIR, BHVO and BCR standards were used as external standards. Si were used as internal standards to correct concentration values. Si concentrations were quantitatively measured

prior to LA-ICP-MS using EPM. Subtraction of gas blanks and internal standard corrections were performed using Thermo Plasmalab software.

Whole-rock major, trace and rare-earth element X-ray fluorescence analyses (XRF) were carried out on a Panalytical PW2404 wavelength-dispersive sequential X-ray spectrometer at the School of Geosciences, University of Edinburgh, U.K. (8 samples). Additional major, trace element and REE bulk rock analyses were obtained by ICP mass spectrometer (Finnigan MAT Element) and ICP atomic emission spectrometry using a Varian Vista AX spectrometer at the Department of Geological Sciences, University of Stockholm, Sweden (6 samples) and at the ACME Analytical Laboratory, Vancouver, Canada (3 samples). For ICP analyses whole-rock powders were decomposed by fusion with lithium metaborate and digestion by nitric acid. Details of the standards used and detection limits are given in the Online Appendix.

5. Mineral chemistry

5.1. Amphibole

According to criteria by Leake et al. (1997) and Hawthorne et al. (2012) amphibole can be classified as kaersutite, pargasite, ferropargasite and magnesio-hastingsite. Magnesium number (Mg#=Mg/(Mg+Fe^{2+})) varies from 0.49 to 0.72, FeO^T and TiO$_2$ contents reach 17.7 wt.% and 5.2 wt.%, respectively, and Al$_2$O$_3$ contents vary in a range of 11.7 and 14.3 wt.% (see Table I of the Supplementary Data).

Cumulus and intercumulus amphiboles have different compositions (Fig. 3). Intercumulus amphibole has higher Mg# and SiO$_2$ contents and lower K$_2$O, FeO^t, Ba (<300 ppm), Sr (<350 ppm) and Zr (<115 ppm) contents than cumulus amphibole crystals (see Table II of the Supplementary Data). Among cumulus crystals, both macrocrysts and microcrysts have similar compositions with high Sr, Ba and Zr concentrations, up to 1850 ppm, 1200 ppm and 560 ppm, respectively. They display a variation trend of increasing Al$_2$O$_3$ and TiO$_2$ and decreasing K$_2$O and FeO^t with increasing Mg#, similar to that of amphibole compositions of the Ditrău camptonites (Batki et al., 2014). Some cumulus amphibole crystal rims are richer in FeO^t and poorer in TiO$_2$ and Mg# than their cores indicating crystallisation towards a slightly more evolved magma or under different conditions (Fig. 3).

Chondrite-normalised (McDonough and Sun, 1995) rare-earth element (REE) patterns for cumulus and intercumulus amphiboles show variable REE enrichment (Fig. 4A). Cumulus amphiboles are 6 to 270 times those of chondrite whilst the intercumulus amphibole is less than 60 times enriched relative to chondritic values. The normalised REE patterns are convex-

upwards for all amphiboles and lack a Eu anomaly. REE patterns, however, display a slight enrichment in Tm-Lu for cumulus amphiboles. La_N/Yb_N ratios are markedly variable with a range from 4.1 to 12.5 (intercumulus amphibole) and from 8.3 to 18.8 (cumulus amphibole). Most trace elements in cumulus and intercumulus amphiboles are 30–300 times enriched compared to chondritic values. Characteristic features of most samples are strong negative anomalies for Th, U, Ta, Pb and Yb and positive anomalies for Ba, Nb, Sr, Zr and Y (Fig.4B).

5.2. Clinopyroxene

The clinopyroxenes range from diopside to augite (ferroan–, and aluminian–ferroan diopside, and Mg-rich augite; Morimoto et al., 1989) with a narrow range of $Di_{51–78}Hd_{15–26}Aeg_{3–8}$ (see Table III of the Supplementary Data).

Two compositional types can be distinguished within clinopyroxene crystals: microcrysts from olivine-bearing cumulates and macrocrysts from pyroxene-rich cumulates (Fig. 5). Clinopyroxene microcrysts have high Mg# $(Mg/(Mg+Fe^{2+})) = 0.77–0.90)$, Al_2O_3 and TiO_2 contents, up to 8.3 wt. % and 2.9 wt.%, respectively, like those of the Ditrău camptonites (Batki et al., 2014). They have variable Cr concentrations (440–5300 ppm), and contain 75–120 ppm Sr and 50–200 ppm Zr (see Table IV of the Supplementary Data). Macrocrysts have somewhat lower Mg# of 0.74–0.84, and are poor in Al_2O_3, TiO_2 and Cr, always below 4.4 wt.%, 1.7 wt.% and 80 ppm, respectively. Macrocrysts are enriched in Sr (200–280 ppm) but similar in Zr (80–210 ppm) compared to microcrysts. Microcrysts together with clinopyroxene microcrysts from olivine-bearing cumulates (Morogan et al., 2000) display a variation trend with decreasing TiO_2, Al_2O_3 and FeO^t and increasing SiO_2 with increasing Mg#. Macrocrysts show a different trend of increasing TiO_2 and Al_2O_3 and decreasing SiO_2 with increasing Mg#, as do the clinopyroxenes of the Ditrău camptonites (Batki et al., 2014). The macrocryst rims are richer in SiO_2 and poorer in TiO_2, Al_2O_3 and Mg# than their cores (Fig. 5). Ti/Al ratios in all clinopyroxene cores fall between 0.125 and 0.250, and below 0.125 indicating a relatively high crystallization pressure.

REE concentrations for clinopyroxenes are 2 to 90 times higher than chondritic values (Fig. 4C). The normalised REE patterns are convex-upwards for all clinopyroxenes and lack a negative Eu anomaly. Although the macrocrysts are richer in REE than the microcrysts, the normalised REE patterns are parallel. La_N/Yb_N values vary between 2.9 and 7.8 (microcrysts) and between 4.7 and 6.5 (macrocrysts).

Most trace elements in clinopyroxenes are 2–200 times enriched relative to chondritic values (Fig. 4D). Strong negative peaks are observed for U and Pb and also for Ta. As in

8

amphiboles, positive anomalies for Nb, Sr, Zr and Y are present. In contrast, normalised Ba and Rb concentrations are variable.

5.3. Other minerals

Relict olivine cores display a narrow range of Fo from 75 to 73 mol%, low CaO (0–0.14 wt.%) and Ni (574–817 ppm), and high MnO contents (0.21–0.43 wt.%, see Table V of the Supplementary Data).

Orthopyroxene occurs as homogeneous enstatite according to criteria by Morimoto et al. (1989) with Mg# ($Mg/(Mg+Fe^{2+})$) of 0.70–0.72 and contains 1.1–1.3 wt.% Al_2O_3, 1–1.3 wt.% CaO and ~180 ppm Ni (see Table VI of the Supplementary Data). Comparison of these Mg- and Al-poor compositions with orthopyroxene crystals from worldwide xenoliths shows that they are similar to crustal granulite xenoliths (e.g. Conticelli, 1998; Nozaka, 1997; Orlando et al., 1994).

Biotite is annite (Mg# = 0.59–0.62), similar to the biotites of the Ditrău camptonites (Batki et al. 2014). As in the clinopyroxenes and amphiboles, high Fe content (FeO^T = 16.7–18.1 wt.%) is a characteristic feature. The biotites have high Al content (Al_2O_3 = 15.3–16.0 wt.%) but low Ti concentrations (TiO_2 = 0.4–1.5 wt.%, see Table VII of the Supplementary Data).

The intercumulus plagioclase ranges from oligoclase to albite, An_{30-2} (seeTable VIII of the Supplementary Data). Some plagioclases in the ultramafic cumulates have relatively K-rich rims (K_2O up to 2.0 wt.%).

6. Whole-rock geochemistry

Major element compositions of four samples of the Ditrău hornblendites were published by Mauritz (1912), Mauritz et al. (1925) and Ianovici (1932, 1933). Morogan et al. (2000) published major and trace element data for six samples. We present here seventeen new geochemical analyses for major and trace elements (Table 1).

6.1. Major elements

Except for the olivine-rich cumulates, the compositions of the amphibole- and pyroxene-rich cumulates overlap, and all the new data accord with those previously published compositions (Ianovici, 1932, 1933; Mauritz, 1912; Mauritz et al., 1925; Morogan et al., 2000; Fig. 6, Table 1). Olivine-rich cumulates are the most primitive with MgO contents of 16.4–16.8 wt.%. All the other mafic–ultramafic cumulates have low SiO_2 but high alkali, TiO_2, P_2O_5 and FeO^T contents (Fig.6, Table 1), consistent with their alkaline character. The K-rich samples can

9

reach up to 4.9 K_2O wt.%. CaO, FeO^T, TiO_2, and P_2O_5 of the cumulates, plotted against Mg# in Fig. 6 show a negative correlation with decreasing Mg#. Conversely SiO_2, Al_2O_3, Na_2O and K_2O decrease as Mg# falls, reflecting the modal rise of amphibole, apatite, titanite and magnetite in the cumulates.

6.2 Trace elements

As with the major elements, the trace element contents of the olivine-rich cumulates differ from the other cumulates (Table 1). They have the highest Ni and Cr contents and are lowest in Sr, Ba, Zr, Nb and Y (Fig.7, Table 1). In contrast, all the other mafic–ultramafic cumulates possess high Sr, Ba, Zr, Nb and Y and lower Ni and Cr (Fig.7, Table 1). Cr, Ni and Sc show a positive correlation with decreasing Mg#, consistent with decreasing olivine and clinopyroxene contents (Fig. 7). Incompatible elements including La, Zr, Sr and Y, together with V increase with decreasing Mg#, reflecting the higher apatite and titanite contents (Fig. 7).

Primitive mantle-normalised trace element patterns of the cumulates are broadly sub-parallel (Fig. 8). Olivine-rich cumulates are the least enriched compared to primitive mantle and characterised by positive Pb, Hf and Ti anomalies and negative Zr and Y anomalies (Fig. 8A). Pyroxene-rich cumulates are depleted in U and K, enriched in P and Ti, and show variable Rb, Th, La-Ce, Pb, Nd and Y contents (Fig. 8B). Additionally, some of the studied cumulates display a Nb enrichment (Fig. 8B, C).

Rare-earth element (REE) patterns have no Eu anomaly and are enriched in light REE relative to the primitive mantle, typical of alkaline rocks, with La/Yb ratios ranging from 5 to 32 (Fig. 8D). These values are similar to those of the Ditrău lamprophyres (La/Yb = 15–38; Batki et al., 2014).

7. Discussion

7.1. Evolution of cumulates

The studied cumulates contain ferromagnesian minerals as cumulus phases but these differ in mineralogy suggesting crystallisation from different melts with different evolutionary histories.

Poikilitic samples contain olivine and clinopyroxene as cumulus phases and they are enclosed by intercumulus amphibole crystals. Ultramafic rocks comprising olivine with compositions $<Fo_{90}$, >0.1 wt.% CaO and <0.3 NiO are generally interpreted to be related to fractional crystallisation of primitive magmas and of not mantle origin (e.g. Stormer, 1973; Pearson et

10

al., 2003; Jankovics et al., 2013; Larrea et al., 2014). The composition of the olivine in the studied cumulates of Fo_{75-73}, ~0.1 wt.% CaO and up to 817 ppm Ni therefore suggests a cumulate origin related to fractional crystallisation of a primitive melt. Poikilitic texture can be interpreted as indicative of closed system crystallisation (e.g. Larocque and Canil, 2010) but it can also indicate open system processes such as recharge (e.g. Tiepolo et al., 2011). The closed system model invokes crystallisation of cumulus olivine and clinopyroxene microcrysts that is followed by amphibole crystallisation from the interstitial melt. Experimental studies of hydrous mafic magmas crystallization indicate that usually olivine and clinopyroxene are the liquidus phases and amphibole saturates after these mineral phases (e.g., Nekvasil et al., 2004; Krawczynski et al., 2012.) in accordance with our textural observations of the poikilitic samples. This closed system evolution suggests that the cumulus minerals have more primitive composition (higher Ni, Cr and MgO contents) than intercumulus phases.

In contrast, the open system evolution model suggests that a former olivine + clinopyroxene-rich crystal mush was replenished by fresh amphibole-forming melt (Tiepolo et al., 2011). In this model intercumulus amphibole indicates a fresh replenishing melt with primitive mineral composition. Both Cr and Ni behave as compatible elements in amphibole and clinopyroxene (Adam and Green, 2006). Cumulus pyroxene microcrysts and intercumulus amphibole in the Ditrău poikilitic cumulates have similar Cr and Ni contents, but clinopyroxene often has much higher Cr content accompanied by higher MgO than amphibole indicating the more primitive nature of the cumulus pyroxene microcrysts (Fig. 3 and 5). Ni content of intercumulus amphibole is somewhat higher than cumulus clinopyroxene microcryst, but this can be the result of the variation of partition coefficient of Ni between melt and adjacent mineral. This is indicated by the #1950 run from the experiments of Adam and Green (2006). They found that $^{Amp/L}D_{Ni}=32\pm3$ and it is much higher than $^{Cpx/L}D_{Ni}=11\pm1$ from the same experiment.

In summary, cumulus minerals especially clinopyroxene have more primitive composition than intercumulus amphibole and this better supports the closed system fractionation model. Although the open system evolution of the poikilitic samples cannot be fully ruled out, mineral chemical data can be interpreted as closed system crystallization. Further combined textural and chemical analyses of the minerals, e.g., clinopyroxene microcrysts, is required to address this issue.

The evolution of the more common amphibole cumulates among the Ditrău mafic-ultramafic cumulates are more clearly the result of closed system crystallisation dominated by the precipitation of clinopyroxene macrocrysts and amphibole cumulus crystals. The cumulus

amphiboles show normal zoning towards their rims as it was shown by Pál-Molnár (2000) that is consistent with closed system evolution. Amphibole crystals contain clinopyroxene inclusions. The clinopyroxene inclusions have the same composition as cumulus clinopyroxene suggesting their common origin (Fig. 4 C, D). This also indicates that the clinopyroxene crystallisation overtakes amphibole crystallisation. Large variation of incompatible elements of cumulus amphiboles from sample to sample (e.g. Zr: 170–560 ppm) is accompanied by Cr content variation of <1–100 ppm (Fig. 9). This suggests that each of the amphibole cumulate samples represents a differently evolved melt batch.

7.2. Estimation of parental melt

The higher compatible and lower incompatible trace element contents of clinopyroxene and amphibole with higher Mg# of poikilitic olivine-rich cumulate samples indicate that they crystallised from more primitive melt than amphibole cumulates.

To determine the Mg# of the possible parental melt the ultramafic cumulates formed from we used mineral-melt equilibrium equations with $Kd^{Fe–Mg}$ values of 0.30 for olivine (Roeder and Emslie, 1970), 0.26 for clinopyroxene (Akinin et al., 2005) and 0.38 for amphibole (LaTourrette et al., 1995). The calculated Mg# of the melts in equilibrium with olivine relict cores vary between 0.45 and 0.47. Magnesium numbers from 0.47 to 0.51 and from 0.42 to 0.58 are calculated for the melts in equilibrium with clinopyroxene microcrysts and macrocrysts, respectively, whereas Mg# of the magmas in equilibrium with intercumulus and cumulus amphibole varies from 0.45 to 0.51 and from 0.26 to 0.36, respectively (Fig. 10A). Such Mg# for the calculated melts in equilibrium with cumulus olivine cores, all clinopyroxene crystals and intercumulus amphibole are very similar to those of the camptonite dykes penetrating the whole complex with whole-rock Mg# of 0.44–0.70 (Batki et al., 2014).

Trace element compositions of the melt in equilibrium with the olivine relict cores was calculated by Kd values determined for alkaline lamprophyre (Arzamastsev et al., 2009) and hydrous basanite melts (Zanetti et al., 2004). $^{Cpx/L}D$ and $^{Amp/L}D$ values determined for camptonite compositions (Ubide et al., 2014) were used to calculate magma compositions in equilibrium with clinopyroxene and amphibole. Chondrite-normalised trace element patterns for the calculated olivine melt are characterised by high Zr, Ti, Y and V contents (Fig. 10B). Magmas in equilibrium with clinopyroxene cumulus crystals have high LREE, Ta and Sr concentrations and a negative Pb anomaly (Fig. 10C). Incompatible trace element patterns of melts in equilibrium with cumulus and intercumulus amphiboles are marked Ba, Nb, Sr and

Zr enrichment and characterised by negative Th, Ta, Pb and Yb anomalies. Except for Th and U, the calculated intercumulus amphibole melt has lower trace element concentrations than that of the cumulus amphibole liquids (Fig. 10D).

7.3. Crystallization conditions

Empirical and experimental studies indicate that the composition of amphiboles can record the crystallization conditions (P, T, fO_2, fH_2O) of magmas (e.g., Johnson and Rutherford, 1989; Ernst and Liu, 1998; Alonso-Perez et al., 2009; Ridolfi et al., 2010; Krawczynski et al., 2012). The studied cumulates contain abundant amphibole crystals suggesting that amphiboles most likely records the temperature and pressure (depth) of the cumulate formation and perhaps one of the main differentiation level in the Ditrău Alkaline Massif. Therefore we used the composition of amphibole to estimate P–T conditions and the depth of magma differentiation.

First we compared the composition of the studied Ditrău cumulate amphiboles with experimentally derived amphiboles from the literature (Fig. 11). This comparison provides a range of P–T conditions within the studied cumulates was formed. The experimental results of alkaline magmas was used for comparison those were reported by Adam et al. (2007), Nekvasil et al. (2004), Caricchi et al. (2006), Freise et al. (2009), Barclay and Carmichael (2004). These experiments represent a broad range of experimental conditions (0.2–2 GPa, 920–1050°C) and magma compositions (SiO_2: 46–56wt.%, MgO: 12–2.7 wt.%). Fig. 11 shows that both cumulus and intercumulus amphiboles of the studied cumulates overlap experimental amphiboles of Nekvasil et al. (2004), Caricchi et al. (2006), Freise et al. (2009) this indicates that the cumulates formed at pressure between 0.4–1 GPa and temperature between 920–1050°C. The cumulus amphiboles from different rock types show overlapping compositions indicating very similar crystallization conditions. On the other hand, intercumulus amphibole have higher Mg# indicating that they were crystallized from more primitive melt than cumulus amphiboles.

Second we calculated P-T conditions applying amphibole thermobarometer. Although several equations exist based on the amphibole composition, but most of them are not calibrated for alkaline magmas except the equations of Ridolfi and Renzulli (2012). The thermobarometer of Ridolfi and Renzulli (2012) is calibrated for large pressure and temperature range. The calculated pressure shows large variations even in a single crystal. Although some compositional variation can be observed in single amphibole crystals, the calculated pressure does not show any relationship with this compositional variation. One example is shown on

Fig. 12, which represents compositional profile across one of the cumulus amphiboles. This crystal shows a flat plateau in the core and progressive compositional change towards its rims. At the same time the calculated pressure fluctuates between 0.5–1.2GPa and this is geologically unrealistic for a single crystal. This suggests that the Ridolfi and Renzulli (2012) barometry is too sensitive for small compositional variations and introduces large uncertainty in the estimation of the depth of magma emplacement.

To overcome this problem we have used an empirical barometer based on the Al_2O_3 content of experimentally produced amphiboles of Adam et al. (2007), Nekvasil et al. (2004), Caricchi et al. (2006), Barclay and Carmichael (2004). The experimental pressures show good correlation with the Al_2O_3 content of experimental amphiboles in the pressure range 0.2–1 GPa (Fig. 13B). Both temperature and melt composition can potentially affect our empirical barometer increasing the uncertainty of the pressure estimation. Therefore we analysed the effect of temperature and melt composition using the extensive experimental dataset of Nekvasil et al. (2004). Fig. 13A shows that effect of pressure on Al_2O_3 content of amphibole has a much higher effect than magma composition or temperature. The uncertainty of the barometer is 190 MPa but in our case it can provide better estimation than the Ridolfi's barometer (Fig. 13C). This Al_2O_3 in amphibole barometer yields a pressure of 0.7±0.05 GPa for both cumulus amphiboles and intercumulus Ditrău amphiboles, that represents approximately 26±2 km depth using average crustal density. The calculated temperatures fall in a narrow range between 1014±24 °C for cumulus and 1024±22 °C for intercumulus amphiboles. These calculated *P–T* conditions suggest that melt emplacement occurred in the lower crust where cumulates was formed during magma differentiation.

7.4. Origin of the Ditrău mafic-ultramafic cumulates

There have been various suggestions concerning the origin of the Ditrău mafic–ultramafic rocks. Kräutner and Bindea (1998) assumed that the ultramafic masses were mantle xenoliths, whilst Morogan et al. (2000) proposed that they could have formed disrupted bodies of former side-wall cumulates. Pál-Molnár (2010b) also supported a cumulate origin for the hornblendites and assumed that their compositions most closely approaches that of their parental magma.

The mineralogy and the mineral compositions suggest that the Ditrău mafic–ultramafic cumulates crystallised from variably evolved, hydrous alkaline mafic melts. Morogan et al. (2000) were the first to propose that the parental melt of Ditrău Alkaline Massif were derived from OIB-like basanitic magmas. Batki et al. (2014) proposed that parental melts of the

massif were similar to the OIB like melts, observed in the late stage camptonite dykes of the complex. The chondrite-normalised trace element patterns for the calculated melts in equilibrium with cumulus pyroxene and amphibole of the amphibole cumulates are consistent with the bulk composition of the Ditrău camptonite dykes (Fig. 10) suggesting that melts similar to late stage camptonites are potential parental melt for those cumulates.

This is also supported by the whole rock compositions. As noted by Davidson et al. (2007) amphiboles can easily fractionate MREE and HREE elements because Dy is more compatible in amphibole than Yb. Thus formation of amphibole cumulates produce an amphibole signal (decreasing Dy/Yb with increasing SiO_2) during magma differentiation. The Ditrău mafic–ultramafic cumulates show large Dy/Yb ratio (Dy/Yb>3.3) larger than the Dy/Yb ratio of the camptonites or other Ditrău magmas (Fig. 14A). The literature data of the Ditrău magmas shows decreasing trend on the SiO_2 vs. Dy/Yb plot suggesting that amphibole crystallization played an important role during magma evolution of the Ditrău Alkaline Massif (Fig .14A). According to this, the studied cumulates represent a lower crustal amphibole "sponge". The amphibole "sponge" model was developed for arc settings (Davidson et al., 2007). However the Ditrău Alkaline Massif represents an intraplate magmatic series, thus amphibole "sponge" can form also in intraplate setting if the primitive magmas are hydrous.

The calculated liquid of cumulus amphiboles has the lowest Mg# and the highest LREE compositions among all calculated melts, it has also higher LREE content than camptonite melts (Fig. 10). This indicates that amphiboles cumulates crystallised from a slightly evolved melt than that of the camptonites. On the other hand, the calculated melt for intercumulus amphiboles show similar pattern to those of the camptonites but the calculated melts have much lower Ba, Sr and Yb contents. This suggests that the poikilitic, olivine-rich cumulate rocks crystallised from OIB like melts but not from the camptonite like melts. The calculated *P–T* conditions, the various Mg# and differences in trace element distributions of the calculated parental melts imply that different magma batches were emplaced in the lower crust and crystallised to form the variable types of mafic–ultramafic cumulates in the Ditrău Alkaline Massif.

The percentage of tetrahedral sites occupied by Al vs. Ti in clinopyroxene (according to Loucks, 1990) clearly follows the trend defined by igneous rocks of continental rifts in general (Fig. 14B), which is in agreement with the intra-plate origin of the Ditrău mafic–ultramafic cumulates. The absence of a significant Nb-Ta negative anomaly in the studied cumulates confirms that a subduction component was not involved in their parental melt generation (Table 1). These results, together with the trace element patterns of the calculated

melts for both cumulate types correspond well with the OIB-like character of the Ditrău magmas (Morogan et al., 2000) and the intra-plate magmatic activity proposed by Pál-Molnár (2010b) and Batki et al. (2014). Preliminary Nd isotope data also support that cumulates were formed from OIB-like melts (Batki et al., 2014). Kräutner and Bindea (1998) assumed an origin associated with a rifted continental margin, while Dallmeyer et al. (1997) proposed that a mantle plume was involved in the generation of the Ditrău rocks.

8. Conclusions

1. Mafic–ultramafic cumulates enclosed in gabbroic–dioritic rocks as lense or block shaped bodies occur in the northern and central-western part of the Ditrău Alkaline Massif. Various ultramafic rock types, olivine-and pyroxene-rich and nearly mono mineralic hornblendite cumulates with typical cumulate textures and geochemical nature are inferred as vertical succession built up on a chamber floor. Field relationships confirm gravitational accumulation. During the Alpine tectonic events the massif was uprooted and most probably tectonically tilted from its original vertical position.

2. Amphibole in the mafic–ultramafic cumulates represent both cumulus and intercumulus phases. Other cumulus minerals include olivine, diopside and augite. These are interpreted to have formed by the accumulation of early crystallising minerals. Decreasing SiO_2 and increasing CaO, FeO^T, TiO_2 and P_2O_5 coupled with decreasing Mg# in bulk rock composition is attributed to abundant titanite, apatite and magnetite crystallisation during accumulation.

3. The Ditrău ultramafic cumulates are inferred to have crystallised from a basanitic parental magma. The calculated Mg# and trace element concentrations of the parental melts indicate the same origin for cumulus olivine and clinopyroxene mush in olivine-rich cumulates crystallising from early lamprophyric melts. Calculations for the parental magma of cumulus clinopyroxene in amphibole- and pyroxene-rich cumulates show that they also crystallised from lamprophyre melts. Compositional differences in calculated parental magmas point to multiple magma batches replenishing the magma chamber. Equilibrium liquids for intercumulus amphibole however, display a more primitive composition than lamprophyres, whereas, cumulus amphibole appear to have crystallised from a more evolved magma than lamprophyres. REE data of the studied ultramafic cumulates suggest an intra-plate

magmatic setting, comparable to an extensional phase of a rifted continental margin and/or a mantle plume.

4. The studied cumulates are proposed to have formed at high temperature and lower crustal levels indicated by the calculated crystallisation conditions of ~T: ~1000-1050 °C and ~P: 0.7 GPa.

References

Adam, J., Green, T., 2006. Trace element partitioning between mica- and amphibole-bearing garnet lherzolite and hydrous basanitic melt: 1. Experimental results and the investigation of controls on partitioning behavior. Contributions to Mineralogy and Petrology 152, 1–17.

Adam, J., Oberti, R., Ca´mara, F., Green, T.H., 2007. An electron microprobe, LAM-ICP-MS and single-crystal X-ray structure refinement study of the effect of pressure, melt-H_2O concentration and fO_2 on experimentally produced basaltic amphiboles. European Journal of Mineralogy 19, 641–655.

Akinin, V.V., Sobolev, A.V., Ntaflos, T., Richter, W., 2005. Clinopyroxene megacrysts from Enmelen melanephelinitic volcanoes (Chukchi Peninsula, Russia): application to composition and evolution of mantle melts. Contributio to Mineralogy and Petrology 150, 85–101.

Alonso-Perez, R., Müntener, O., Ulmer, P., 2009. Igneous garnet and amphibole fractionation in the roots of island arcs: experimental constraints on andesitic liquids. Contribution to Mineralogy and Petrology 157, 541–558.

Armstrong, J.T., 1991. Quantitative elemental analysis of individual microparticles with electron beam instruments, in: Heinrich, K.F.J., Newbury, D.E. (Eds.), Electron Probe Quantitation. Plenum Press, New York, pp 261–315.

Arzamastsev, A.A., Arzamastseva, l.V., Bea, F., Montero, P., 2009. Trace elements in minerals as indicators of the evolution of alkaline ultrabasic dike series: LA-ICP-MS data for the magmatic provinces of northeastern Fennoscandia and Germany, Petrology 17, 46–72.

Bagdasarian, G.P., 1972. Despre virsta absolută a unor roci eruptive și metamorfice din masivul Ditrău și Munții Banatului din Romania. [Absolute age of eruptive and metamorphic rocks from Ditrău and Banat Mountains in Romania.] Studii şi Cercetări Geologie, Geofizică, Geografie, Seria Geologie 17/1, 13–21.

Barclay, J., Carmichael, I.S.E., 2004. A hornblende basalt from western Mexico: water-saturated phase relations constrain a pressure–temperature window of eruptibility. Journal of Petrology 45, 485–506.

Batki, A., Pál-Molnár, E., Dobosi, D., Skelton, A., 2014. Petrogenetic significance of ocellar camptonite dykes in the Ditrău Alkaline Massif, Romania. Lithos 200–201, 181–196.

Caricchi, L., Ulmer, P., Peccerillo, A., 2006. A high-pressure experimental study on the evolution of the silicic magmatism of theMain Ethiopian Rift. Lithos 91, 46–58.

Conticelli, S., 1998. The effect of crustal contamination on ultrapotassic magmas with lamproitic affinity: mineralogical, geochemical and isotope data from the Torre Alfina lavas and xenoliths, Central Italy. Chemical Geology 149, 51–81.

Codarcea, A., Codarcea, D.M., Ianovici, V., 1957. Structura geologică masivului de roci alcaline de la Ditrău. [Geological structure of alkaline rocks from the Ditrău Massif.] Buletinul Ştiinţific al Academiei Republicii Populare Române, Secţia de Geologie şi Geografie II/3–4, 385–446.

Davidson, J., Turner, S., Handley, H., MacPherson, C., Dosseto, A., 2007. Amphibole ''sponge'' in arc crust? Geology 35, 787–790.

Dallmeyer, D.R., Kräutner, H.G., Neubauer, F., 1997. Middle-late Triassic 40Ar/39Ar hornblende ages for early intrusions within the Ditrau alkaline massif, Rumania: Implications for Alpine rifting in the Carpathian orogen. Geologica Carpathica 48, 347–352.

Eby, GN., 1984. Monteregian Hills I. Petrography, major and trace element geochemistry, and strontium isotopic chemistry of The Western Intrusions: Mounts Royal, St. Bruno, and Johnson. Journal of Petrology 25/2, 421–452.

Ernst, W.G., Liu, J., 1998. Experimental phase-equilibrium study of Al- and Ti-contents of calcic amphibole in MORB-A semiquantitative thermobarometer. American Mineralogist 83, 952–969.

Fall, A., Bodnar, R.J., Szabó, Cs., Pál-Molnár, E., 2007. Fluid evolution in the nepheline syenites of the Ditrău Alkaline Massif, Transylvania, Romania. Lithos 95, 331–345.

Freise, M., Holtz, F., Nowak, M., Scoates, J.S., Strauss, H., 2009. Differentiation and crystallization conditions of basalts fromthe Kerguelen large igneous province: an experimental study. Contribution to Mineralalogy and Petrolology 158, 505–527.

Hawthorne, F.C., Oberti, R., Harlow, G.E., Maresch, W.V., Martin, R.F., Schumacher, J.C., Welch, M.D., 2012. Nomenclature of the amphibole supergroup. American Mineralogist 97, 2031–2048.

Herbich, F., 1859. Die geologischen Verhältnisse des nordöstlichen Siebenbürgens. Jahrb. Ungarn geol Anstalt, 293–350.

Hoeck, V., Ionescu, C., Koller, F., 2006. Mesozoic ophiolites in the Dinarides and the Carpathians: a review. Acta Mineralogica-Petrographica, Abstract Series 5, 39–41.

Hoeck, V., Ionescu, C., Balintoni, I., Koller, F., 2009. The Eastern Carpathians "ophiolites" (Romania): Remnants of a Triassic ocean. Lithos 108, 151–171.

Ianovici, V., 1932. Gabbro á olivine provenant de Pârâul Jolotca, Ditrău, district Ciuc. Ann. Scient. Univ. Jassy 18, 107–112.

Ianovici, V., 1933. Étude sur le massif syénitique de Ditrău, région Jolotca, district Ciuc (Transylvanie). Rev. Muz. Geol. Min. Univ. Cluj 4/2, 1–53.

Ianovici, V., 1938. Considérations sur la consolidation du massif syénitique de Ditrău, en relation avec la tectonique de la région. C. R. Acad. Sci. Roum II/6, 689–694.

Irvine, T.N., Baragar, W.R.A., 1971. A guide to the chemical classification of the common volcanic rocks. Canadian Journal of Earth Sciences 8, 523–548.

Jakab, Gy., 1998. Geologia Masivului alcalin de la Ditrău. [Geology of Alkaline Massif from Ditrău.] Pallas-Akademia, Miercurea-Ciuc, 298 p. (in Romanian).

Jankovics, M.É., Dobosi, G., Embey.Isztin, A., Kiss, B., Sági, T., Harangi, Sz., Ntaflos, T., 2013. Origin and ascent history of unusually crystal-rich alkaline basaltic magmas from the western Pannonian Basin. Bulletin of Volcanology 75:749.

Johnson, M.C., Rutherford, M.J., 1989. Experimentally determined conditions in the Fish Canyon Tuff, Colorado magma chamber. Journal of Petrology 30/3, 711–737.

19

Kozur, H., 1991. The evolution of the Meliata-Hallstatt ocean and its significance for the early evolution of the Eastern Alps and Western Carpathians Palaeogeography, Palaeoclimatology, Palaeoecology 87/1–4, 109–135.

Krawczynski, M., Grove, T., Behrens, H., 2012. Amphibole stability in primitive arc magmas: effects of temperature, H_2O content, and oxygen fugacity. Contributions to Mineralogy and Petrology 164/2, 317–339.

Kräutner, H.G., Bindea, G., 1995: The Ditrău alkaline intrusive complex and its geological environment. Romanian Journal of Mineralogy 77/3, 1–44.

Kräutner, H.G., Bindea, G., 1998. Timing of the Ditrău alkaline intrusive complex (Eastern Carpathians, Romania). Slovak Geological Magazine 4, 213–221.

Larocque, J., Canil, D., 2010. The role of amphibole in the evolution of arc magmas and crust: the case from the Jurassic Bonanza arc section, Vancouver Island, Canada. Contribution to Mineralogy and Petrology 159, 475–492.

Larrea, P., Galé, C., Ubide, T., Widom, E., Lago, M., França, Z., 2014. Magmatic evolution of Graciosa (Azores, Portugal). Journal of Petrology, doi:10.1093/petrology/egu052.

LaTourrette, T., Hedvig, R.L., Holloway, J.R., 1995. Trace element partitioning between amphibole, phlogopite, and basanite melt. Earth and Planetary Science Letters 135, 13–30.

Leake, B.E., Woolley, A.R., Arps, C.E.S., Birch, W.D., Gilbert, M.C., Grice, J.D., Hawthorne, F.C., Kato, A., Kisch, H.J., Krivovichev, V.G., Linthout, K., Laird, J., Mandarino, J.A., Maresch, W.V., Nickel, E.H., Rock, N.M.S., Schumacher, J.C., Smith, D.C., Stephenson, N.C.N., Ungaretti, L., Whittaker, E.J.W., Youzhi, G., 1997. Nomenclature of Amphiboles: Report on the Subcommittee on Amphiboles of the International Mineralogical Association, Commission on New Minerals and Mineral Names. American Mineralogist 82, 1019–1037.

Loucks, R.R., 1990. Discrimination of ophiolitic from nonophiolitic ultramafic-mafic allochthons in orogenic belts by the Al/Ti ratio in clinopyroxene. Geology 18, 346–349.

Mauritz, B., 1912. Adatok a gyergyó-ditrói szienittömzs kémiai viszonyainak ismeretéhez. [Data for the knowledge of chemistry of the Ditrău Syenite Massif). Matematikai Természettudományi Értesítő 30, 607–631. (in Hungarian).

Mauritz, B., Vendl, M., Harwood, H.F., 1925. A ditrói szienit további petrokémiai vizsgálata. [Further petrochemical examination of the Ditrău syenite.] Matematikai Természettudományi Értesítő 41, 61–73. (in Hungarian).

McDonough, W.F., Sun, C., C., 1995. Composition ot the earth. Chemical Geology 120, 223–253.

Morimoto, N., Fabries, J., Ferguson, A.K., Ginzburg, I.V., Ross, M., Seifert, F.A., Zussman, J., Aoki, K., Gottardi, G., 1989. Nomenclature of pyroxenes. Subcommittee on Pyroxenes. American Mineralogist 73, 1123–1133.

Morogan, V., Upton, B.G.J., Fitton, J.G., 2000. The petrology of the Ditrău alkaline complex, Eastern Carpathians. Mineralogy and Petrology 69, 227–265.

Nekvasil, H., Dondolini, A., Horn, J., Filiberto, J., Long, H., Lindsley, D.H., 2004. The origin and evolution of silica-saturated alkalic suites:an experimental study. Journal of Petrology 45, 693–721.

Nozaka, T., 1997. Structure and development of the lower crust and upper mantle of Southwestern Japan: Evidence from petrology of deep-seated xenoliths. Island Arc 6/4, 404–420.

Orlando, A., Conticelli, S., Manetti, P., Vaggelli, G., 1994. The basement of the Northern Vulsinian Volcanic District as inferred from the study of crustal xenoliths from the Torre Alfina lavas Viterbo, Central Italy. Mem. Soc. Geol. Italiana 48, 681–688.

Pál-Molnár, E., 1992. Petrographical characteristics of Ditró (Orotva) hornblendites, Eastern Charpatians, Transylvania (Romania): a preliminary description. Acta Mineralogica-Petrographica 33, 67–80.

Pál-Molnár, E., 1994. A Ditrói Szienitmasszivum kialakulása a földtani megismerés tükreben. [Formation of the Ditrău Syenite Massif in view of geological aspects.] A Magyar Tudomanyos Akademia Szegedi Akademiai Bizottsaganak Kiadvanyai, Szeged, 85 p. (in Hungarian).

Pál-Molnár, E., 2000. Hornblendites and diorites of the Ditrău Syenite Massif. Department of Mineralogy, Geochemistry and Petrology, University of Szeged (Ed.), Szeged, 172 p.

Pál-Molnár, E. 2010a. Geology of Székelyland, in: Szakáll, S., Kristály, F. (Eds.), Mineralogy of Székelyland, Eastern Transylvania, Romania, Csík County Nature and Conservation Society, Sfântu Gheorghe, Miercurea Ciuc, Târgu Mureş, pp 33–43.

Pál-Molnár, E., 2010b. Rock-forming minerals of the Ditrău Alkaline Massif, in: Szakáll, S., Kristály, F. (Eds.), Mineralogy of Székelyland, Eastern Transylvania, Romania, Csík County Nature and Conservation Society, Sfântu Gheorghe, Miercurea Ciuc, Târgu Mureş, pp 63–88.

Pál-Molnár, E., Árva-Sós, E., 1995. K/Ar radiometric dating on rocks from the northern part of the Ditrău Syenite Massif and its petrogenetic implications. Acta Mineralogica-Petrographica 36, 101–116.

Pearson, D.G., Canil, D., Shirey, S.B., 2003. Mantle sample included in volcanic rocks: xenoliths and diamonds, in: Carlson, R.W. (Ed.), Treatise on Geochemistry: the Mantle and Core. Elsevier, pp 171–276.

Ridolfi, F., Renzulli, A., Puerini, M., 2010. Stability and chemical equilibrium of amphibole in calc-alkaline magmas: an overview, new thermobarometric formulations and application to subduction-related volcanoes. Contribution to Mineralogy Petrology 160, 45–66.

Ridolfi, F., Renzulli, A., 2012. Calcic amphiboles in calc-alkaline and alkaline magmas: thermobarometric and chemometric empirical equations valid up to 1,130 °C and 2.2 GPa. Contributions to Mineralogy and Petrology 163, 877–895.

Roeder, P.L., Emslie, R.F., 1970. Olivine-Liquid equilibrium. Contribution to Mineralogy and Petrology 29, 275–289.

Săndulescu, M., 1984. Geotectonica Rômâniei. [Geotectonics of Romania.] Editura Tehnică, Bucureşti, 336 p. (in Romanian).

Săndulescu, M., Kräutner, H.G., Balintoni, I., Russo-Săndulescu, M., Micu, M., 1981. The Structure of the East Carpathians (Moldavia – Maramures Area). Guide Exc. B1, XII Congress of the Carpathian Balkan Geological Association, Inst. Geol. Geophys., Bucuresti, 92 p.

Smith, D.J., 2014: Clinopyroxene precursors to amphibole sponge in arc crust. Nature Communications 5, 4329.

Stormer, J.C., 1973. Calcium zoning in olivine and its relationship to slica activity and pressure. Geochimica et Cosmochimica acta 37, 1815–1821.

Streckeisen, A., 1952, Das Nephelinsyenit-Massiv von Ditro (Siebenburgen), I. Teil. Schweizerische Mineralogische und Petrographische Mitteilungen 32, 251–308.

Streckeisen, A. 1954. Das Nephelinsyenit-Massiv von Ditro (Siebenburgen), II. Teil. Schweizerische Mineralogische und Petrographische Mitteilungen 34, 336–409.

Streckeisen, A. 1960. On the structure and origin of the Nephelinesyenite Complex of Ditro (Transylvania, Roumania). Rep. 21th IGC 13, 228–238.

Streckeisen, A., Hunziker, J.C., 1974. On the origin of the Nephelinsyenit Massif of Ditro (Transylvania, Romania). Schweizerische Mineralogische und Petrographische Mitteilungen 54, 59–77.

Sun, S., Mcdonough, W.F., 1989. Chemical and isotopic systematics of ocean basalts implications for mantle composition and process in: Saunders, A.D., Norry, M.J. (Eds.), Magmatism in the ocean basins. Geological Society Special Publication 42, 313–346.

Tiepolo, M., Tribuzio, R., Langone, A. 2011. High-Mg andesitepetrogenesis by amphibole crystallization and ultramafic crust assimilation: Evidence from Adamello hornblendites (Central Alps, Italy). Journal of Petrology 49, 937-970.

Ubide, T., Galé, C., Arranz, E., Lago, M., Larrea, P., 2014. Clinopyroxene and amphibole crystal populations in a lamprophyre sill from the Catalonian Coastal Ranges (NE Spain): A record of magma history and a widow to mineral-melt partitioning. Lithos 184-187, 225–242.

Upton, B.G.J., Parsons, I., Emeleus, C.H., Hodson, M.E., 1996. Layered alkaline igneous rocks of the Gardar Province, South Greenland. In: Cawthorn, C.G. (ed.): Layered intrusions 331–363. Elsevier Science B.V

Zanetti, A., Tiepolo, M., Oberti, R., Vannucci, R., 2004. Trace-element partitioning in olivine: modeling of a complete data set from a synthetic hydrous basanitic melt. Lithos 75, 39–54.

Figure captions

Fig. 1. (A) Location of the Ditrău Alkaline Massif in the structural system of the Alpine–Carpathian–Dinaric region (Pál-Molnár, 2010a). (B) Alpine structural units of the Eastern Carpathians (Săndulescu et al., 1981, modified) (C) Schematic geological map of the Ditrău Alkaline Massif (Batki et al., 2014). (D) Sample locations in the northern part of the Ditrău Alkaline Massif with the same legend as in figure C.

Fig. 2. Characteristic cumulate features of the studied mafic–ultramafic cumulates from the Ditrău Alkaline Massif. (A) Cumulus amphiboles showing adcumulate texture in hornblendite VRG7433, +N. (B) Olivine, clinopyroxene and magnetite enclosed in the intercumulus amphibole in olivine-rich cumulate VRG23b, +N.(C) BSE image of orthopyroxene containing magnetite inclusion in olivine-rich cumulate VRG23b. (D) BSE image of large diopside crystal up to 4 mm in size in amphibole- and pyroxene-rich cumulate VRG6706. (E) Clinopyroxene and magnetite enclosed in amphibole showing poikilitic texture in amphibole- and pyroxene-rich cumulate VRG7452, +N. (F) Cumulus amphibole and titanite with intercumulus plagioclase displaying mesocumulate texture in amphibole-rich cumulate VRG6546, +N. (G) Titanite crystals containing apatite inclusions in amphibole- and pyroxene-rich cumulate VRG6706, +N. (H) Apatite and magnetite crystals enclosed in amphibole grains in amphibole-rich cumulate VRG7437, +N.

Fig. 3. Compositional trends in amphibole for the Ditrău mafic–ultramafic cumulates. Ol CM: olivine-rich cumulate, Px CM: pyroxene-rich cumulate, Am CM: amphibole-rich cumulate.

Fig. 4. Chondrite-normalised (McDonough and Sun, 1995) trace element and REE variation diagrams of cumulus and intercumulus phases of the Ditrău mafic–ultramafic cumulates. (A) REE patterns for cumulus and intercumulus amphiboles. (B) Trace element patterns for cumulus and intercumulus amphiboles. (C) REE patterns for clinopyroxene cumulus crystals. (D) Trace element patterns for clinopyroxene cumulus crystals.

Fig. 5. Compositional variations in clinopyroxene for the Ditrău mafic–ultramafic cumulates.

Fig. 6. Correlation diagrams for selected whole-rock major elements vs. Mg# for the Ditrău mafic–ultramafic cumulates.

Fig. 7. Correlation diagrams of selected whole-rock trace elements vs. Mg# for the Ditrău mafic–ultramafic cumulates.

Fig. 8. Plots of trace element abundances normalised to primitive mantle (Sun and McDonough, 1989) for (A) olivine-rich cumulate (B) pyroxene-rich cumulate (C) amphibole-rich cumulate and (D) Primitive mantle-normalised (Sun and McDonough, 1989) REE diagram showing moderately to steeply sloping pattern for all of the Ditrău mafic–ultramafic cumulates. Ditrău lamprophyres (Batki et al., 2014) and OIB (Sun and McDonough, 1989) shown for comparison.

Fig. 9. Trace element plots of amphibole and clinopyroxene (cpx) crystals from the Ditrău mafic–ultramafic cumulates. (A) Cr vs Zr plot. (B) Cr vs Ni plot. The variation of cumulus amphibole data represents sample to sample differences.

Fig. 10. Calculated melts in equilibrium with mineral phases of the Ditrău mafic–ultramafic cumulates. (A) Calculated Mg# of melts in equilibrium with cumulus and intercumulus crystals. (B, C and D) Chondrite-normalised (McDonough and Sun, 1995) trace element distribution for melts in equilibrium with olivine, clinopyroxene and amphibole.

Fig. 11. Comparison of literature experimental amphibole data with the Ditrău cumulate amphiboles. We used only the experimental results of alkaline starting materials for the comparison. The grayscale fields (#1-5) represents the compositions of experimental amphiboles from five different publications. The numbers represent the following conditions: #1: 0.4-0.9 GPa, 920-1040°C; #2: 0.5-0.1GPa, 950-1050°C; #3: 0.2 GPa, 1000-1035°C; #4: 09 0.5GPa, 950-1040°C; 5: 1-2 GPa, 1000-1050°C. The references of the experiments #1: Nekvasil et al. (2004); #2: Caricchi et al. (2006); #3: Barclay & Carmichael (2004); #4: Freise et al (2009); 5: Adam et al. (2007).

Fig. 12. (A) Compositional profiles across a cumulus amphibole from sample VRG6547. (B) Calculated pressure profiles of the same crystal. R2012: the pressure profile was calculated with Ridolfi and Renzulli (2012) barometry. Al_2O_3 in amph: the pressure profile was calculated with the barometer of this study based on the Al_2O_3 content of experimental amphiboles. (see text for details)

Fig. 13. (A) The Al_2O_3 (wt.%) vs MgO (wt.%) diagram of experimental amphiboles. The plot shows the effect (indicated by blue arrows) of pressure (p) temperature (T) and magma composition (Xmelt) on amphibole composition. Data are from Nekvasil et al. (2004). A, B, C represents different starting materials as it is expressed by their MgO (wt.%) content. (B) Correlation of Al_2O_3 (wt.%) of experimental amphiboles with pressure (data from Nekvasil et al., 2004; Caricchi et al., 2006; Barclay and Carmichael, 2004; Adam et al., 2007). We used only the experimental results of alkaline starting materials. The method of Ridolfi et al. (2010) was used for data selection. (C) Empirical Al_2O_3 in amph barometer reproducibility of experimental pressure. The plot shows the calculated vs. experimental pressure, and 1:1 line. The standard deviation from the 1:1 line is also shown. The test includes the experiments of the alkaline starting materials of Freise et al. (2009), Nekvasil et al. (2004); Caricchi et al. (2006); Barclay and Carmichael (2004); Adam et al., (2007).

Fig. 14. (A) Bulk rock SiO_2 vs. Dy/Yb plot of the Ditrău magmas. (B) Compositional variations of Al^{IV} (in percent of total tetrahedral cations) vs. TiO_2 in clinopyroxene of cumulates from the Ditrău Alkaline Massif. Trends for cumulates and volcanic rocks from different tectonic settings are after Loucks (1990).
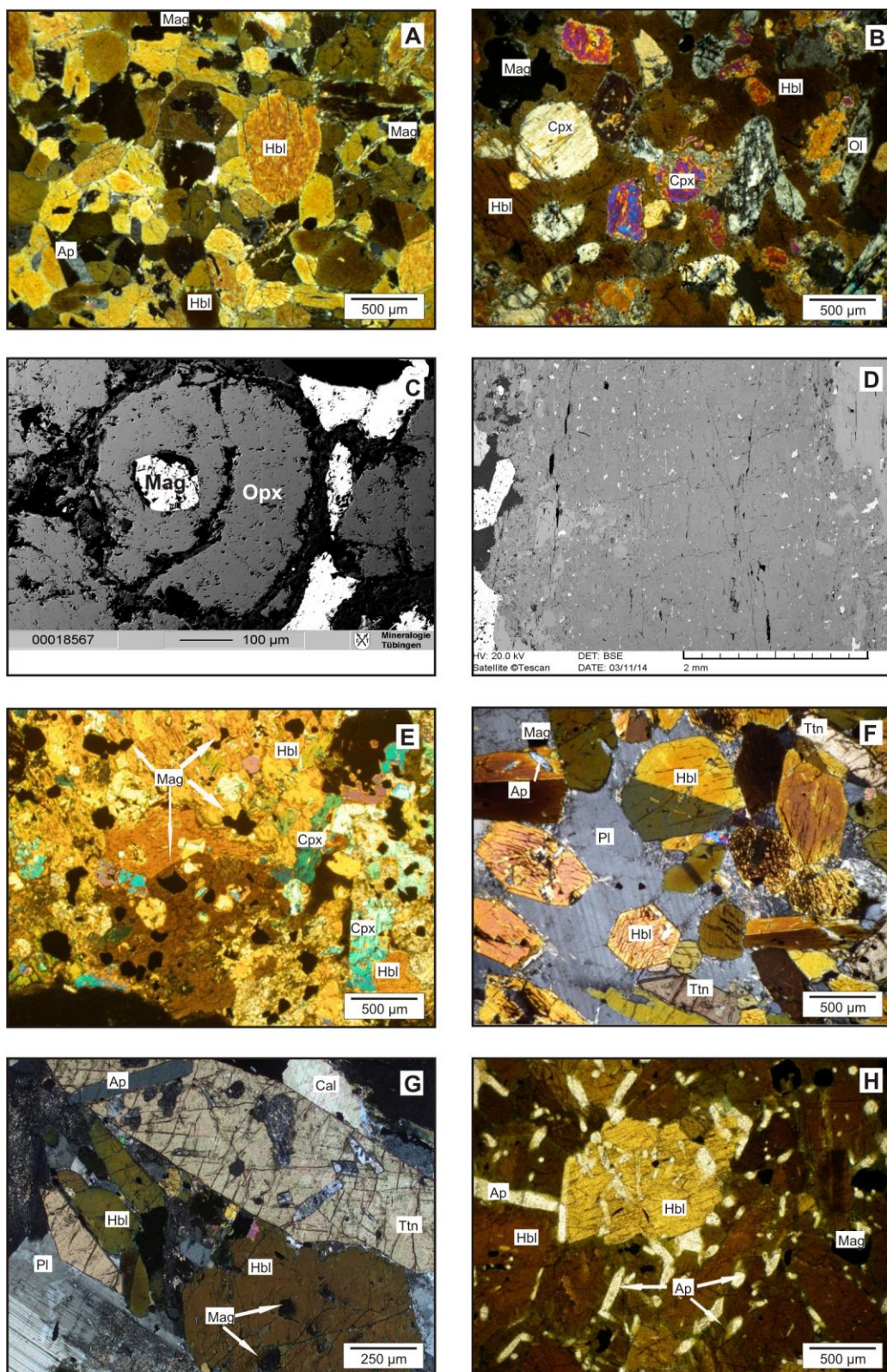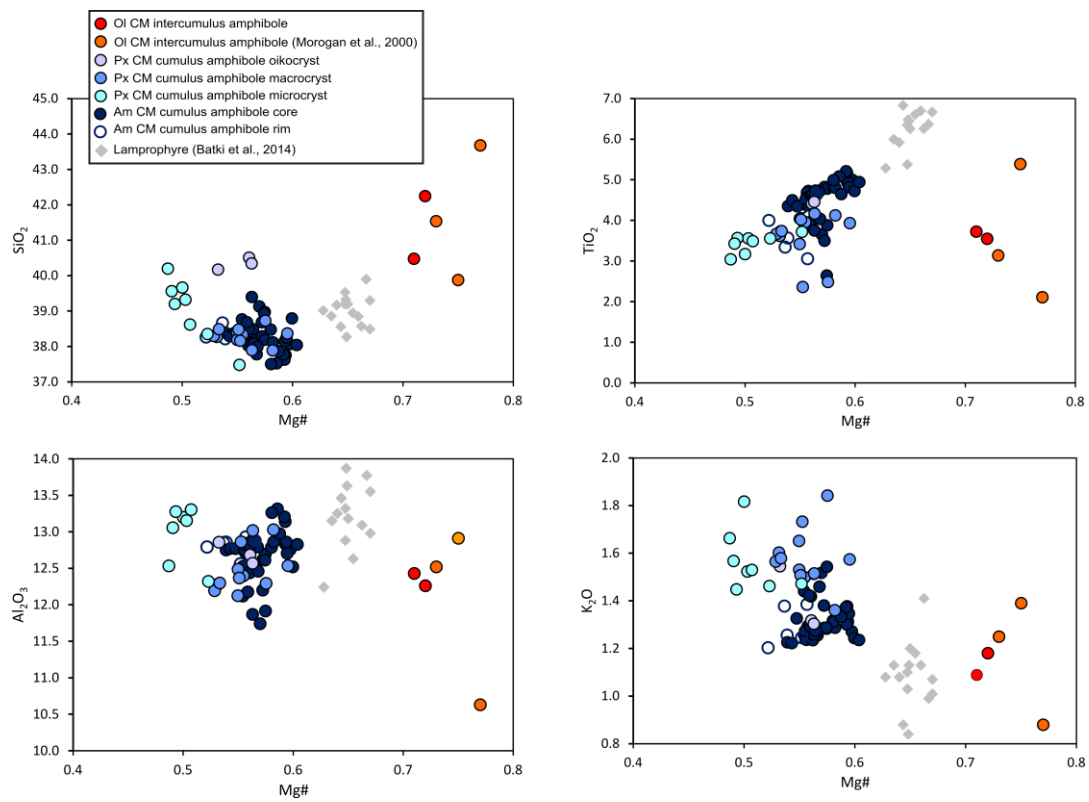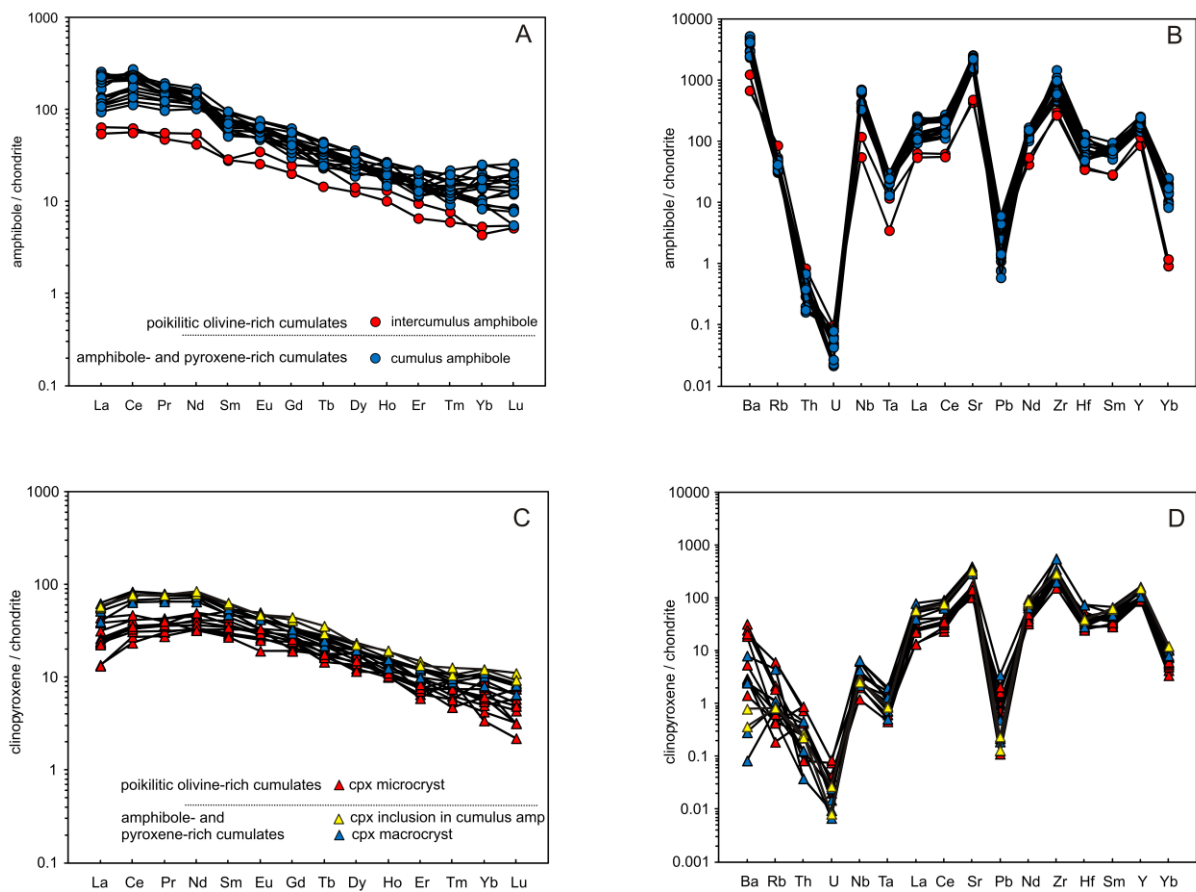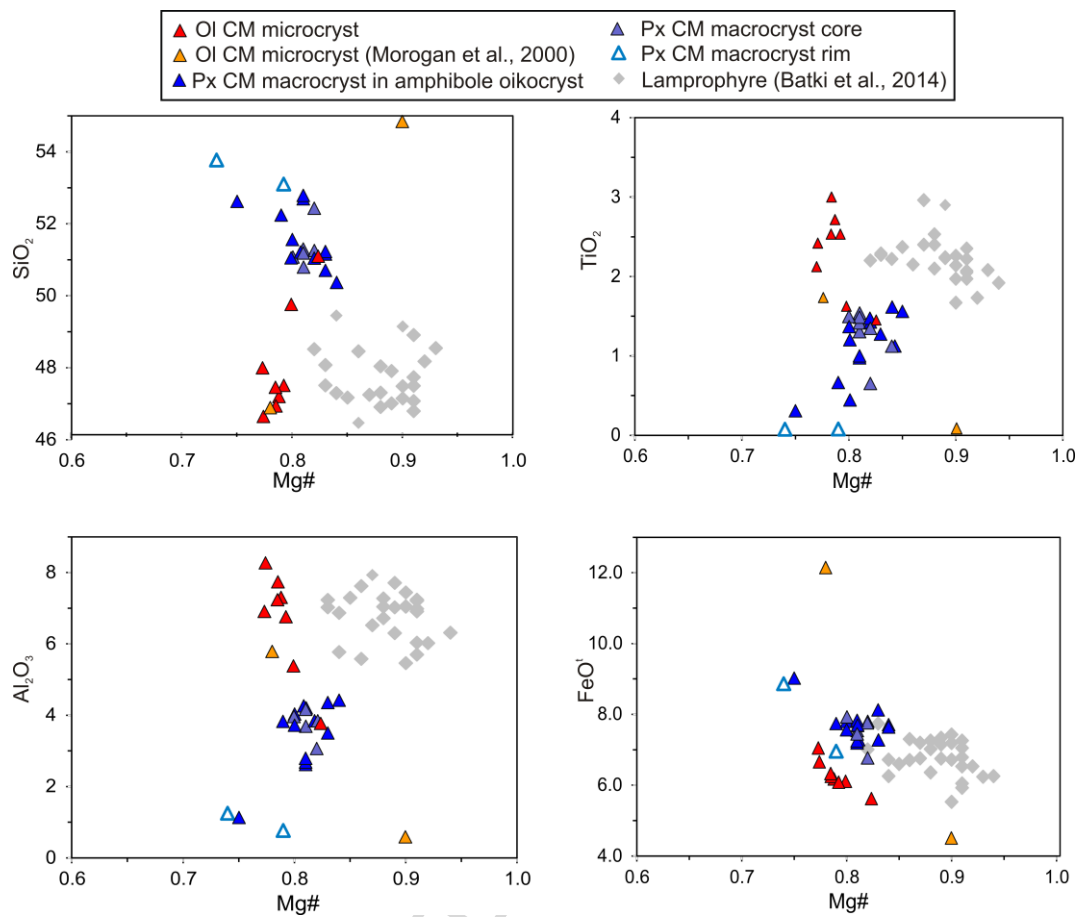
Figure 1

Figure 2

Figure 3
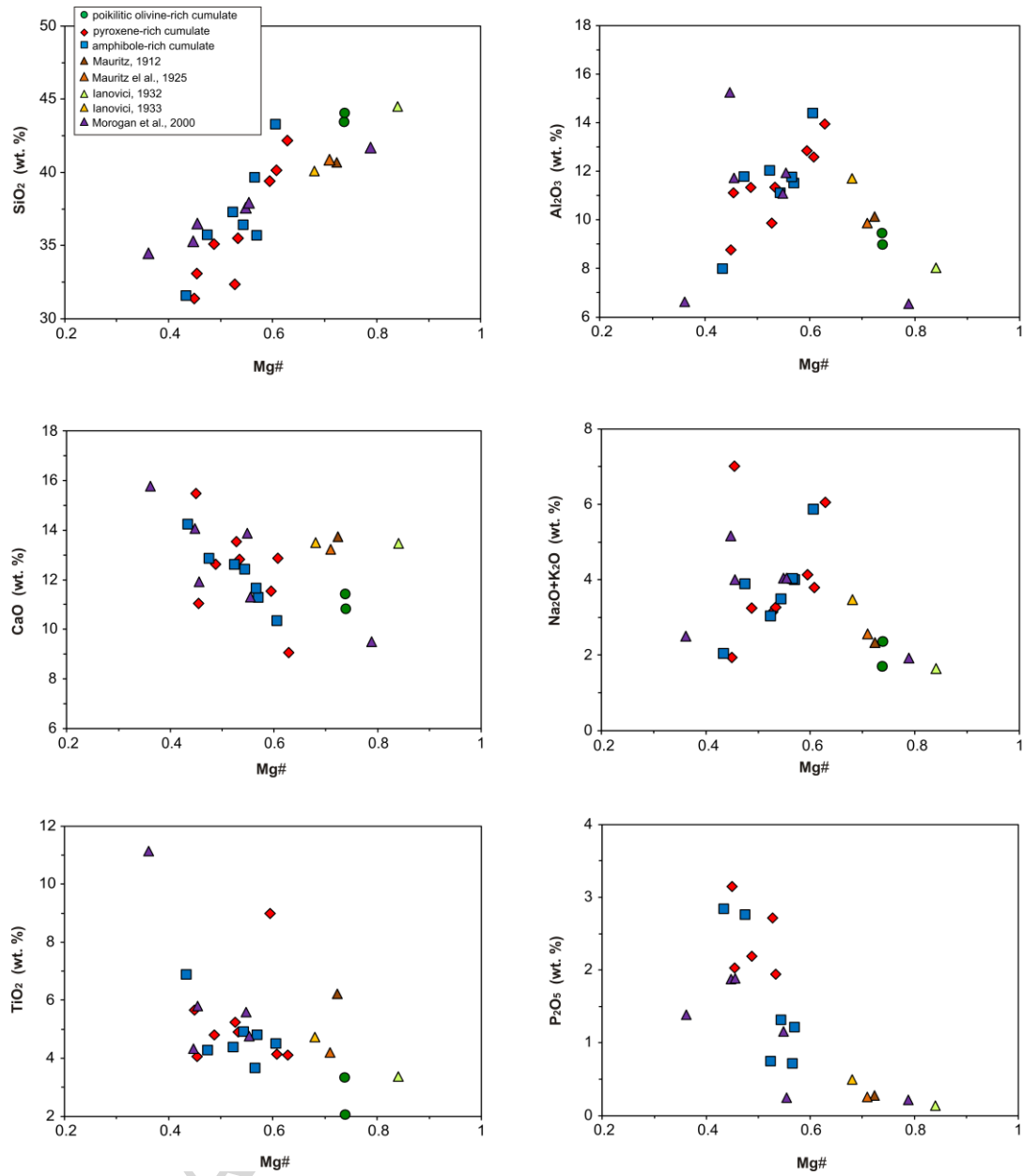
Figure 4

Figure 5

Figure 6
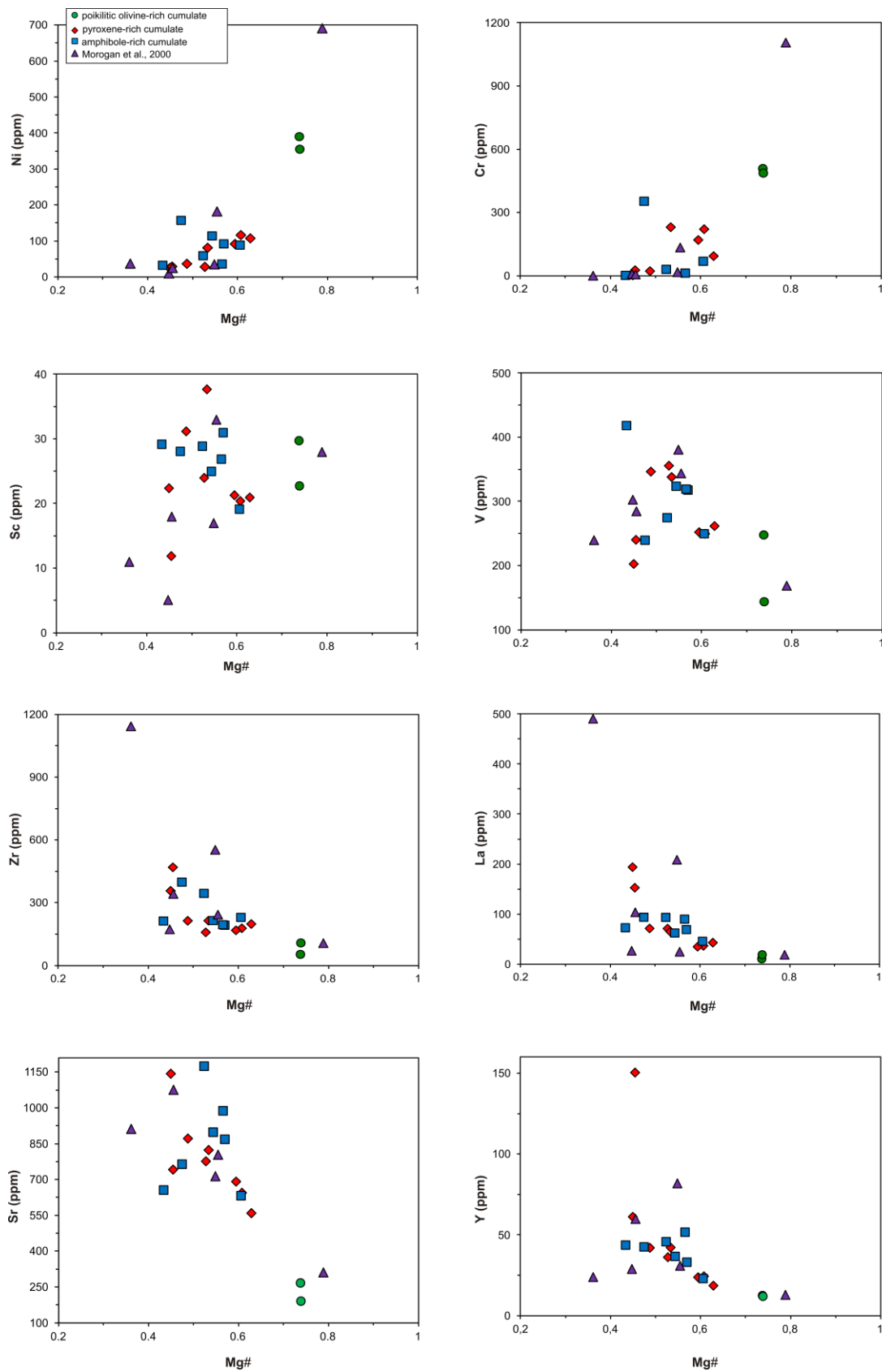
Figure 7
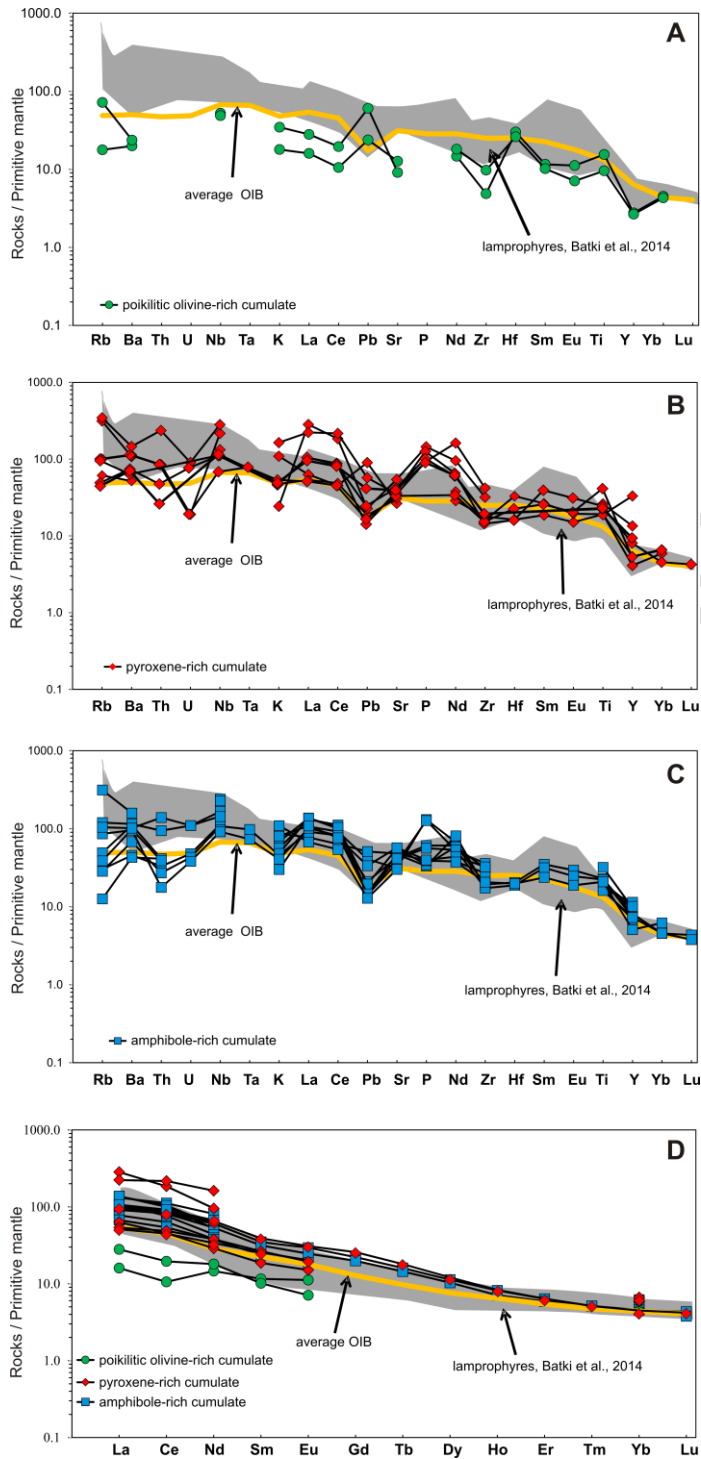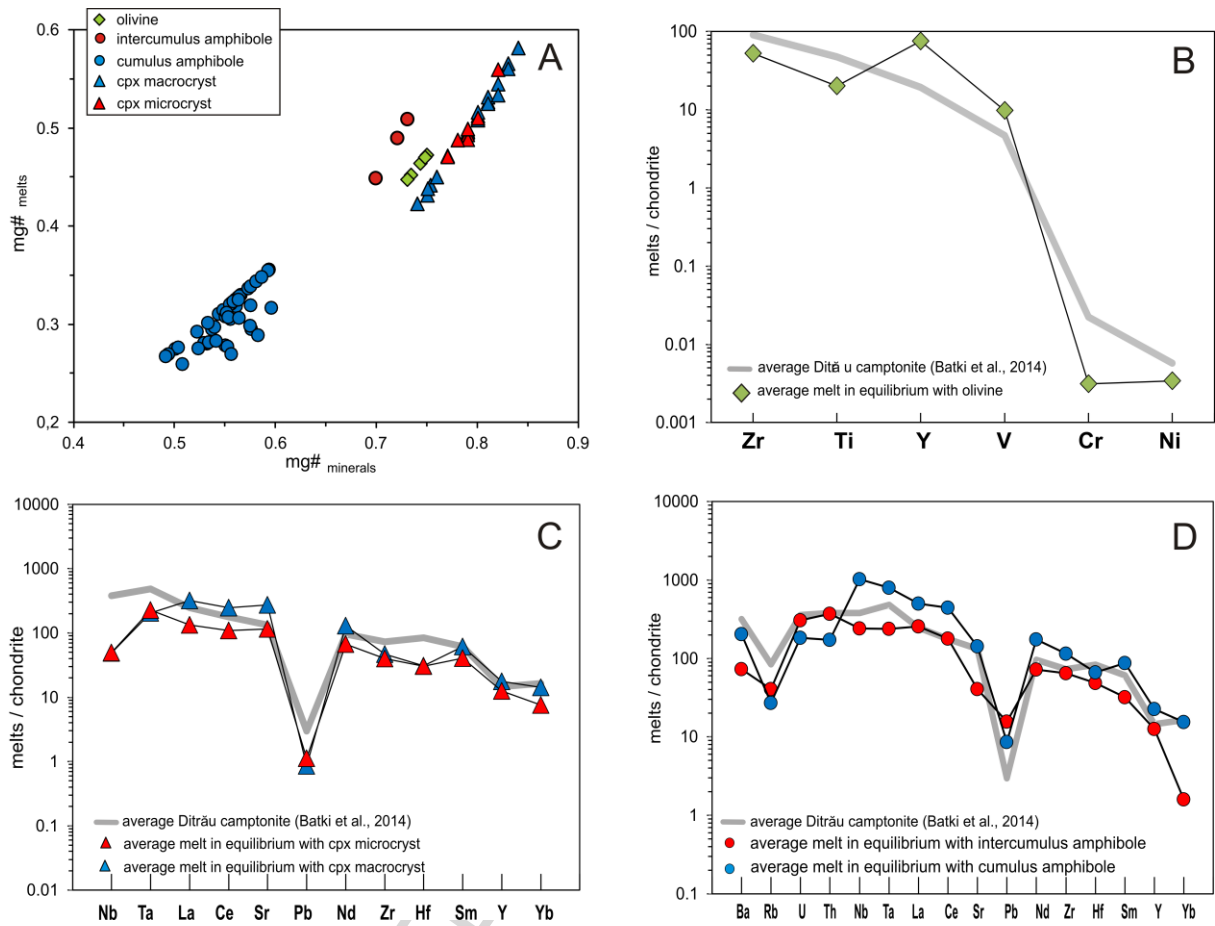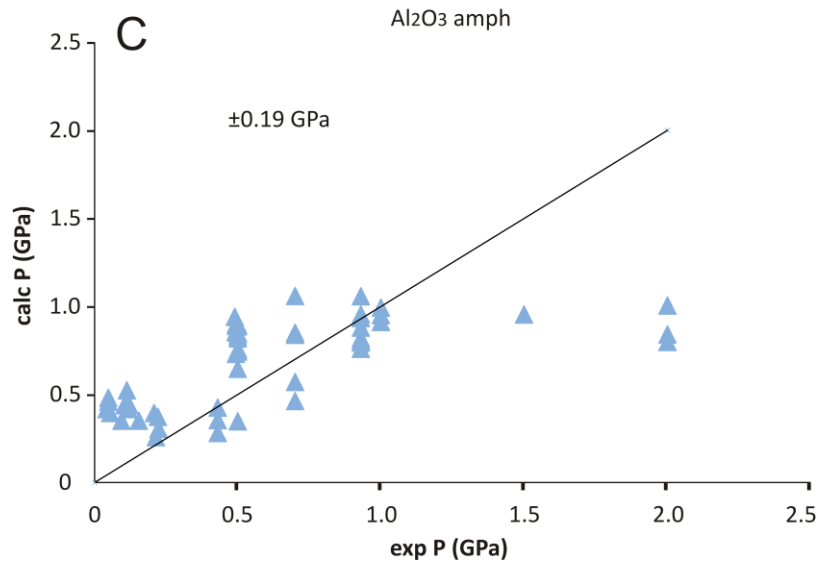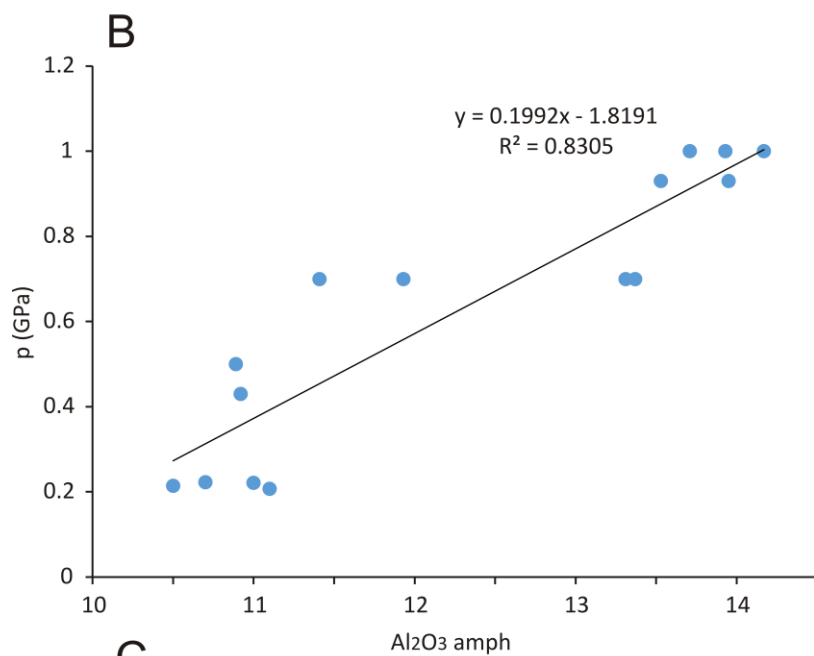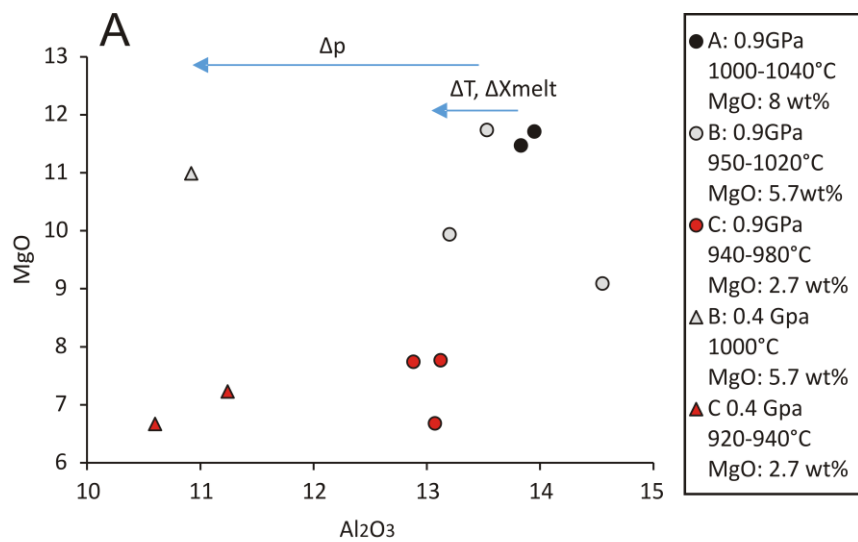
Figure 8
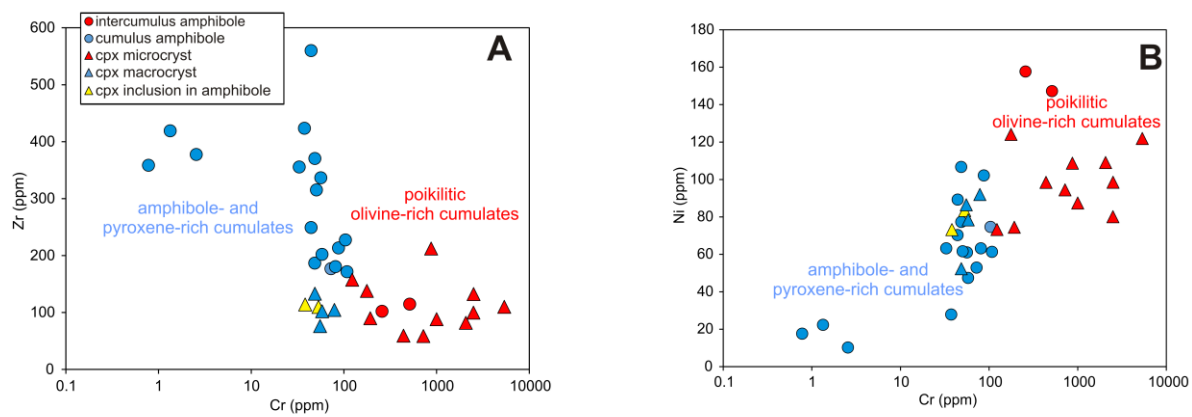
Figure 9
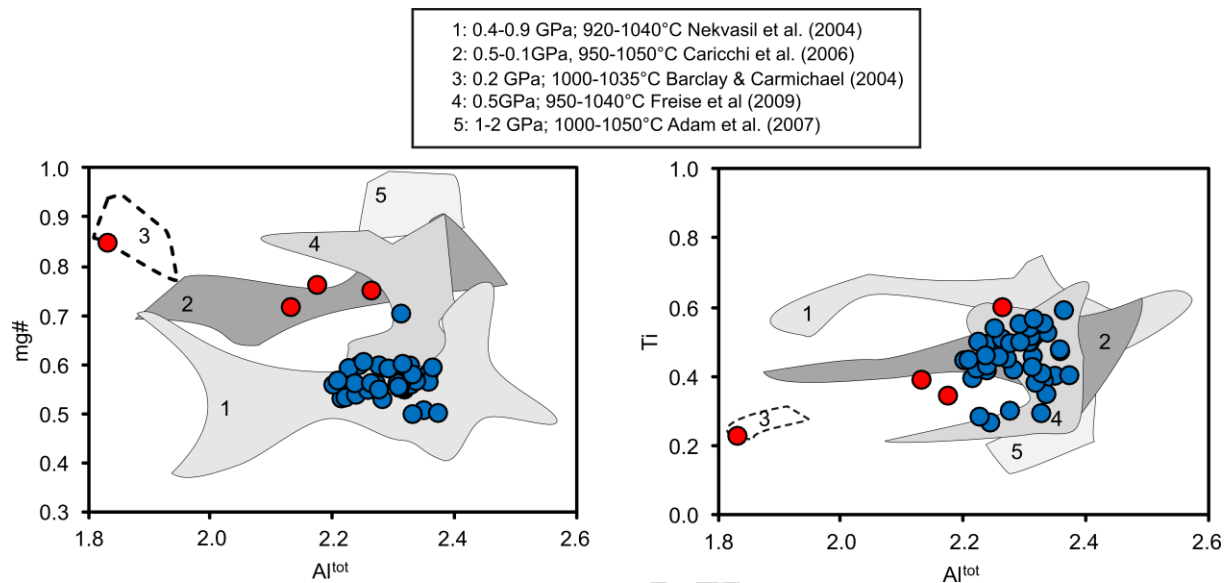
Figure 10

Figure 11
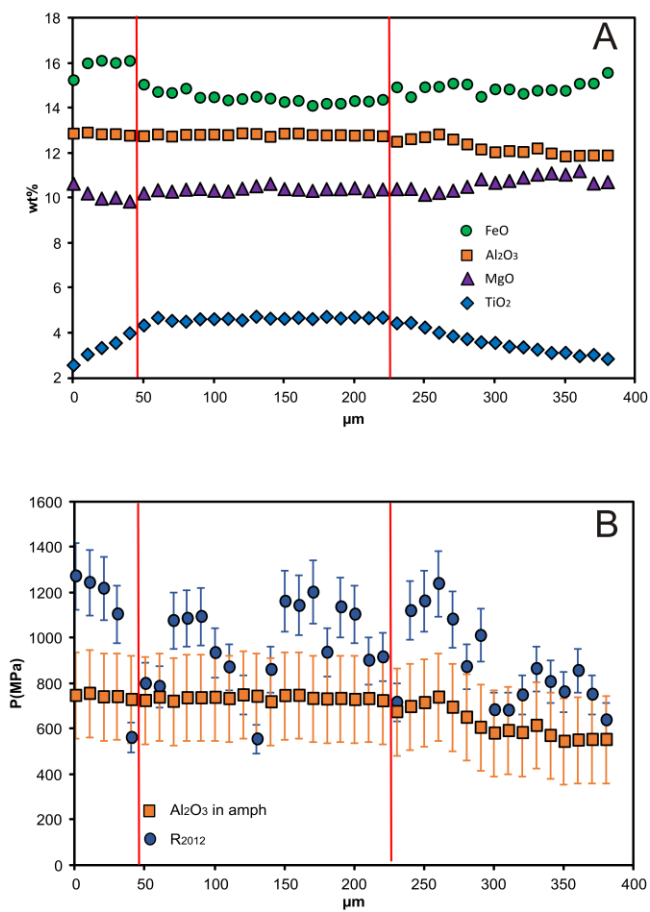
Figure 12

Figure 13
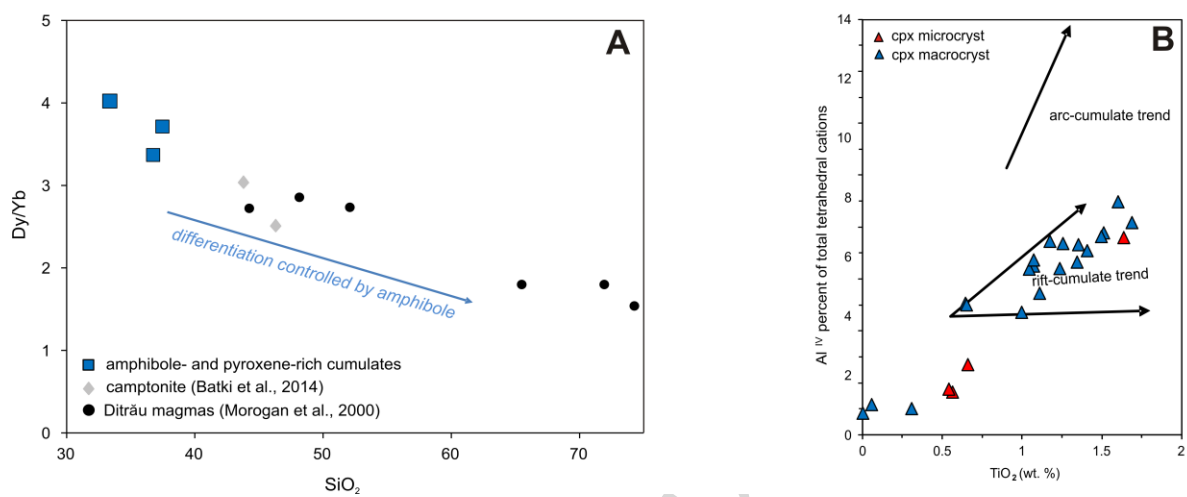
Figure 14

Table 1. Whole-rock analyses of mafic-ultramafic cumulates from the Ditrău Alkaline Massif

Sample	VRG6749	VRG6757	VRG6710	VRG6713	VRG7452	VRG7450	VRG6706	VRG6546	VRG7432	VRG7428
wt. %	Olivine-rich cumulate		Pyroxene-rich cumulate							
SiO_2	43.46	44.07	42.18	40.15	31.39	33.09	32.36	39.41	35.11	35.51
Al_2O_3	9.47	9.00	13.96	12.60	8.78	11.13	9.88	12.86	11.35	11.36
TiO_2	3.35	2.07	4.12	4.15	5.67	4.07	5.25	9.00	4.81	4.91
Fe_2O_3	2.90	2.35	2.81	3.29	2.25	1.59	4.24	3.05	1.94	1.78
FeO	11.77	10.11	10.61	13.02	20.19	14.29	16.89	11.49	17.44	16.02
FeO^T	14.67	12.46	13.42	16.31	22.44	15.89	20.73	14.54	19.39	17.81
MgO	16.82	16.40	10.59	10.57	9.23	6.68	9.06	9.65	9.30	10.26
MnO	0.17	0.19	0.19	0.25	0.32	1.04	0.26	0.23	0.26	0.23
CaO	11.44	10.84	9.07	12.88	15.49	11.06	13.55	11.55	12.64	12.83
Na_2O	1.17	1.33	2.77	2.37	1.21	2.08	1.77	2.54	1.85	1.81
K_2O	0.54	1.04	3.29	1.43	0.73	4.94	1.38	1.60	1.41	1.47
P_2O_5	—	—	—	—	3.15	2.03	2.72	—	2.19	1.95
LOI	—	—	—	—	1.46	7.65	2.60	—	1.26	1.27
Total	101.09	97.40	99.59	100.71	99.88	99.66	99.56	101.38	99.56	99.40
mg#	0.74	0.74	0.63	0.61	0.45	0.45	0.53	0.59	0.49	0.53
ppm										
Be	0.24	0.67	1.30	1.11	—	—	—	1.07	—	—
Sc	29.76	22.76	20.97	20.42	22.40	11.90	24.00	21.32	31.20	37.70
V	248.15	144.14	261.97	250.00	202.90	240.60	356.00	252.53	346.80	338.40
Cr	509.44	487.90	94.09	221.79	2.50	27.40	—	170.65	22.90	231.40
Co	76.81	63.25	52.14	46.46	—	—	63.20	46.47	—	—
Ni	390.03	355.06	107.33	116.29	24.60	28.90	28.00	91.65	36.50	81.00
Cu	141.71	131.82	16.86	41.27	63.00	9.00	57.80	44.34	38.10	51.10
Zn	90.05	108.59	131.49	156.55	278.20	391.80	142.00	146.66	208.90	189.80
Sr	267.93	191.86	560.30	645.63	1144.30	742.70	777.50	692.49	872.80	824.70
Ba	139.34	165.13	754.20	363.33	788.40	1023.00	418.00	441.55	514.20	489.30
Rb	11.27	45.59	199.25	38.88	63.60	219.40	28.80	60.12	31.00	28.10
Zr	54.50	109.08	199.45	179.10	358.00	470.30	159.60	169.36	214.80	215.30
Pb	4.40	11.17	16.70	3.42	4.20	10.60	2.60	3.02	4.50	7.60
Nb	37.27	34.70	94.62	78.83	154.30	201.00	48.40	79.24	78.50	81.90
Y	12.58	12.09	18.69	24.50	61.30	150.60	36.30	23.90	42.10	42.30
Hf	9.27	8.05	5.02	10.15	—	—	4.90	6.91	—	—
Ta	—	—	—	—	—	—	3.20	—	—	—
La	10.97	19.19	43.25	36.79	194.30	153.10	71.40	35.06	71.70	65.30
Ce	18.72	34.64	80.58	86.44	327.50	383.80	155.30	79.60	150.90	142.80
Pr	—	—	—	—	—	—	20.28	—	—	—
Nd	19.82	24.43	38.99	51.37	128.90	219.30	88.20	45.68	81.10	82.70
Sm	5.14	4.51	8.29	11.75	—	—	17.32	11.34	—	—
Eu	1.88	1.19	2.53	3.26	—	—	5.18	3.40	—	—
Gd	—	—	—	—	—	—	15.33	—	—	—
Tb	—	—	—	—	—	—	1.94	—	—	—
Dy	3.33	3.89	4.20	6.21	—	—	8.89	6.12	—	—
Ho	—	—	—	—	—	—	1.36	—	—	—
Tm	—	—	—	—	—	—	0.38	—	—	—
Er	—	—	—	—	—	—	3.07	—	—	—

W	—	—	—	—	—	—	1.10	—	—	—
Lu	—	—	—	—	—	—	0.31	—	—	—
Yb	2.22	2.12	2.91	3.28	—	—	2.21	3.18	—	—
U	—	—	—	—	0.40	1.90	—	1.00	1.60	—
Th	—	—	—	—	7.20	20.10	2.70	—	4.00	2.20
ΣREE	104.42	124.82	220.41	244.02	734.40	918.70	452.57	229.60	377.00	370.80

Mg#: Mg/(Mg+Fe^{2+}), Fe^{2+} calculated according to Irvine and Baragar (1971) (continued)

Table 1. continued

Sample	VRG6745	VRG6547	VRG6755	VRG7431	VRG7433	VRG7451	VRG7453
wt. %	Amphibole-rich cumulate						
SiO$_2$	43.30	36.43	35.71	31.59	37.31	39.67	35.74
Al$_2$O$_3$	14.41	11.13	11.53	8.01	12.05	11.78	11.80
TiO$_2$	4.52	4.93	4.82	6.90	4.40	3.68	4.29
Fe$_2$O$_3$	3.13	3.68	3.66	2.30	1.75	1.56	1.82
FeO	11.89	14.32	14.34	20.69	15.72	14.00	16.37
FeO^T	15.02	17.65	17.66	23.04	17.48	15.56	18.20
MgO	9.65	9.54	10.63	8.88	9.69	10.19	8.29
MnO	0.22	0.26	0.29	0.33	0.41	0.39	0.35
CaO	10.36	12.44	11.30	14.26	12.63	11.67	12.88
Na$_2$O	2.59	2.12	1.91	1.15	1.60	2.35	1.86
K$_2$O	3.29	1.38	2.10	0.90	1.45	1.69	2.04
P$_2$O$_5$	—	1.32	1.22	2.85	0.75	0.72	2.77
LOI	—	2.30	2.30	1.35	2.02	2.04	1.24
Total	103.36	99.50	99.47	99.25	99.78	99.75	99.46
mg#	0.61	0.54	0.57	0.43	0.52	0.57	0.47
ppm							
Be	1.29	1.00	1.00	—	—	—	—
Sc	19.16	25.00	31.00	29.20	28.90	26.90	28.10
V	250.02	324.00	318.00	418.60	275.00	319.60	239.90
Cr	69.74	—	—	2.70	31.30	13.60	354.50
Co	46.70	56.60	52.60	—	—	—	—
Ni	88.49	114.00	92.00	32.50	59.00	35.90	157.10
Cu	44.04	45.00	34.50	55.30	12.60	39.30	16.50
Zn	141.97	119.00	154.00	221.50	298.90	247.30	236.40
Sr	633.29	899.40	869.70	657.10	1176.00	988.90	765.30
Ba	1104.76	476.00	669.00	317.80	683.30	298.90	775.20
Rb	198.87	18.00	54.50	19.20	24.60	8.00	31.20
Zr	230.90	215.90	193.50	213.70	345.80	195.90	399.60
Pb	2.37	3.90	2.70	7.50	3.60	2.80	2.60
Nb	101.86	76.70	65.10	80.70	162.20	69.00	170.30
Y	23.11	36.80	33.20	43.80	45.90	51.80	42.70
Hf	6.11	6.30	5.80	—	—	—	—
Ta	—	4.00	3.00	—	—	—	—
La	46.12	62.60	69.40	73.10	93.80	90.30	94.10
Ce	95.81	145.20	144.50	162.70	184.40	197.70	177.30
Pr	—	18.68	17.63	—	—	—	—
Nd	50.51	82.20	72.30	90.70	79.20	109.50	70.90
Sm	10.52	15.50	13.98	—	—	—	—
Eu	3.16	4.92	4.13	—	—	—	—
Gd	—	13.20	11.84	—	—	—	—

Tb	—	1.73	1.56	—	—	—	—
Dy	5.38	8.32	7.58	—	—	—	—
Ho	—	1.34	1.16	—	—	—	—
Tm	—	0.38	0.38	—	—	—	—
Er	—	3.06	2.83	—	—	—	—
W	—	1.20	0.60	—	—	—	—
Lu	—	0.32	0.28	—	—	—	—
Yb	3.05	2.24	2.25	—	—	—	—
U	—	0.90	0.70	1.00	—	0.00	—
Th	—	2.30	1.50	2.80	3.30	3.50	3.50
ΣREE	256.82	422.69	414.62	399.50	432.20	476.20	413.10

Mg#: $Mg/(Mg+Fe^{2+})$, Fe^{2+} calculated according to Irvine and Baragar (1971)

43

45

Highlights

1. Ditrău cumulates are interpreted as vertical succession
2. Ditrău lamprophyres are deduced to reflect the parental magma
3. Multiple magma batches replenished the magma chamber
4. Geochemical data are consistent with an intra-plate petrogenesis
5. The cumulates are supposed to have emplaced at lower crustal levels

47